Reviewed Preprint
v1 • March 11, 2026
Not revised

Reviewed Preprint
v2 • May 6, 2026
Revised by authors

Molecular architecture of the tumor microenvironment caused by *BRCA1* and *BRCA2* somatic mutations in lung adenocarcinoma

Gaoming Liao[1,2,†], Xinbin Yang[1,†], Qi Liu[2,†], Shufeng Nan[2], Yan Liu[3], Jinwei Li[3], Si Huang[3], Wang Ning[1], Xionghai Qin[4], Gang Xu[1]

[1]Guangzhou Institute of Cancer Research, the Affiliated Cancer Hospital, Guangzhou Medical University, Guangzhou, China • [2]State Key Laboratory of Respiratory Disease, National Clinical Research Center for Respiratory Disease, National Center for Respiratory Medicine, The First Hospital of Guangzhou Medical University, Guangzhou, China • [3]Guangzhou Medical University, Guangzhou, China • [4]Department of Thoracic Surgery, Harbin Medical University Cancer Hospital, Harbin, China

For correspondence:
lgm179496478@163.com
qxh9069@163.com
xugang1973@126.com

† Gaoming Liao, Xinbin Yang, and Qi Liu contributed to this work as first author.

Competing interests: No competing interests declared

Funding: See page 22

Reviewing editor: Jia Wei, Department of Oncology, Nanjing Drum Tower Hospital, Affiliated Hospital of Medical School, Nanjing University, Nanjing, China., China

eLife Assessment

This **important** study investigates the impact of BRCA1/2 mutations on immunotherapy in lung adenocarcinoma using multi-omics approaches. The detailed genetic analysis of two cancer genes (BRCA1 and BRCA2) demonstrated their new roles in causing the tumor microenvironment in lung cancer. The **solid** findings of this study provide an essential foundation for further developing drugs targeting BRCA1/2 in lung cancer therapy.

https://doi.org/10.7554/eLife.110662.2.sa3

Abstract

Objectives Homologous recombination repair (HRR) deficiency is associated with improved immunotherapy responses in non-small cell lung cancer (NSCLC) patients. The HRR genes *BRCA1/2* are key regulators of DNA repair, yet their impact on the tumor microenvironment (TME) in lung adenocarcinoma (LUAD) remains unclear.

Methods Using single-cell sequencing and multi-omics data, we characterized *BRCA1/2* mutation-associated transcriptional programs, immune cell composition, and functional alterations in T cells, investigating the molecular and immune architecture of BRCA-mutant LUAD patients.

Results *BRCA1/2* mutations were associated with increased genomic instability and poor prognosis in LUAD patients, but predicted better clinical outcomes following immune checkpoint blockade (ICB) treatment. *BRCA1* mutations correlated with an upregulated type I IFN/IFN-γ signature and $CD8^+$ T cell activation. *BRCA2* mutations were associated with alveolar/stress/inflammatory responses and enhanced MHC-II antigen presentation, linked to $CD4^+$ T cell differentiation. Both alterations coincided with reduced CD28 co-stimulation and CTL activity, hinting of immune evasion. We identified two tissue-resident memory T cell (Trm) subsets as predictors of clinical outcomes and ICB response. *BRCA1* mutations were associated with $CD8^+$ Trm expansion, whereas *BRCA2* mutations linked to tumor $CD4^+$ Trm expansion and peripheral T/NK cell cytotoxicity. Furthermore, a cancer-promoting program activated by *BRCA1* mutation was vulnerable to histone deacetylase inhibitors, which inhibited LUAD tumor growth.

Conclusions This study provides a preliminary characterization of the BRCA-mutant TME in LUAD patients, revealing distinct transcriptional and immune patterns that highlight differences

in *BRCA1/2*-associated molecular architecture and offer a framework for improving therapy efficacy in LUAD.

1. Introduction

Lung adenocarcinoma (LUAD), the most common histological subtype of non-small cell lung cancer (NSCLC), remains a leading cause of cancer-related mortality worldwide [1]. The genetic landscape of this disease is complex, involving multiple driver mutations such as *EGFR*, *KRAS*, and genomic instability alterations, which collectively contribute to tumor progression and metastasis [2–4]. The tumor microenvironment (TME) plays a critical role in shaping tumor progression, immune evasion, and therapeutic response, particularly in the context of genetic mutations affecting DNA repair mechanisms [5, 6]. Homologous recombination repair (HRR) deficiency, characterized by mutations in key DNA repair genes, has been increasingly recognized as a determinant of tumor genomic instability in breast cancer, ovarian cancers, and lung cancer [7–9].

BReast CAncer gene 1 (*BRCA1*) and gene 2 (*BRCA2*) are crucial mediators of genomic stability, and their mutations often lead to increased DNA damage, heightened immune surveillance, and altered tumor-immune interactions [10, 11]. Previous studies revealed that mutations in *Brca1* and *Brca2* mediate distinct immune microenvironment effects in murine models of breast cancer, and showed that *Brca2* deficiency improved response to immune checkpoint inhibitors [10, 12]. Among the key genetic mutations that drive LUAD, *BRCA1* and *BRCA2* mutations (with prevalence rates of approximately 4% and 5%, respectively) have been increasingly implicated in the pathogenesis and progression of lung cancer [9, 13]. Recent studies suggest that HRR-deficient tumors exhibit distinct immunogenic profiles, influencing immune cell infiltration, antigen presentation, and responses to immune checkpoint blockade (ICB) therapy in NSCLC [14, 15]. *BRAC1* mRNA can predict the efficacy of second-line cisplatin chemotherapy in patients with metastatic NSCLC and has a good predictive value for patients with advanced NSCLC receiving platinum-based chemotherapy [16, 17]. One report showed a case of *BRCA2*-positive lung adenocarcinoma, in which the disease was stable for about 2 years after treatment with olaparib [18]. Despite this, the molecular architecture of the TME in LUAD with *BRCA1* and *BRCA2* mutations remains incompletely understood. Understanding the molecular mechanisms through which *BRCA1* and *BRCA2* mutations alter the TME in LUAD is crucial for identifying potential therapeutic targets and improving treatment strategies. To address these challenges, we leveraged single-cell RNA sequencing (scRNA-seq) and single-cell T cell receptor sequencing (scTCR-seq) to comprehensively dissect the *BRCA1/2*-driven TME in LUAD. scRNA-seq enables transcriptomic profiling at the single-cell level, providing unparalleled insights into cellular heterogeneity, lineage differentiation, and gene expression dynamics within tumors [19, 20]. Unlike bulk RNA sequencing, which averages gene expression across heterogeneous cell populations, scRNA-seq allows for the identification of distinct malignant and immune cell subsets, as well as their functional states [21]. Furthermore, scTCR-seq offers a powerful approach for understanding T cell diversity, clonal expansion, and antigen-specific immune responses [22].

In this study, we leveraged large-scale genomic and transcriptomic datasets to investigate the prognostic implications of *BRCA1/2* mutations in LUAD patients (Nearly 2,000 samples). By integrating scRNA-seq and scTCR-seq, this study provides a high-resolution characterization of the immune microenvironment and antigen-specific T cell responses in *BRCA1/2*-mutant LUAD. Our findings reveal how *BRCA1/2* mutations shape the immune landscape, influence $CD8^+$ and $CD4^+$ T cell populations, and modulate immunotherapy outcomes. These insights offer comprehensive view of the molecular mechanisms underlying *BRCA1* and *BRCA2* mutations in LUAD and highlights new opportunities for personalized therapeutic strategies.

2. Materials and methods

2.1. Human specimens

Patient-derived samples for this study were collected at Affiliated Cancer Hospital & Institute of Guangzhou Medical University, Guangdong, China. All patients were treatment-naïve and had invasive lung adenocarcinoma and PD-L1 negative confirmed based on immunohistochemistry. Fresh tumor and adjacent normal tissues of patients were collected through surgery. This study was approved by the Ethics Committee of Affiliated Cancer Hospital and Institute of Guangzhou Medical University (Approval No. KY-2025003) in compliance with the international guidelines. All patients have signed informed consent. The samples were divided into two parts, one for single-cell sequencing and the other for whole exome sequencing. In addition, we collected and obtained public datasets of multiple cohorts. The genomic variation, gene expression, and clinical data of LUAD patients (n=564) of the cancer genome atlas (TCGA) program were downloaded from cBioPortal data resource (*https://www.cbioportal.org/*). The genomic variation and survival data of LUAD in individuals of East Asian ancestry (OncoSG cohort, n=305) [23] also from cBioPortal. The mutation and survival data of LUAD patients receiving ICB treatment from SU2C MARK cohort (n=309) [24]. The gene expression, survival, and response data of NSCLC patients receiving ICB treatment from OAK cohort (n=699) [25]. Tumor mutation burden (TMB), homologous recombination deficiency (HRD) score, and neoantigen load data for TCGA-LUAD patients were obtained from a previous study [26]. The HRD score was determined by summing specific genomic alterations, including loss of heterozygosity (LOH), large-scale state transitions (LST), and telomeric allelic imbalances (TAI). Tumor mutation burden (TMB) was defined as the total number of somatic nonsynonymous mutations per megabase of the exome captured by the sequencing panel. Neoantigen load was predicted by NetMHCpan using the patient's HLA typing and the identified somatic mutations.

2.2. DNA extraction and library construction of whole exome sequencing

Genomic DNA were extracted from lung adenocarcinoma tissues and blood using CretMag^{TM} Multi Sample DNA Kit. Genomic DNA were captured using Agilent SureSelect Human All Exon v6 library following the manufacturer's protocol (Agilent Technologies, USA). DNA libraries were constructed following the protocols provided by Illumina. Then these libraries were sequenced on the Illumina sequencing platform (Illumina NovaSeq X plus) and 150 bp paired-end reads were generated. The whole exome sequencing was conducted by OE Biotech Co., Ltd. (Shanghai, China).

2.3. Somatic variant identification

The raw reads (fastq) of whole exome sequencing were pre-processed and trimmed with fastp (Version: 0.23.4) based on default parameters. Clean reads were aligned to the reference human genome (GRCh38) utilizing the BWA (version 0.7.17). The mapped reads were sorted and indexed by using SAMtools (Version 1.5). The GATK (Version 4.0.5.1) was used for recalibration of the base quality score and for single nucleotide polymorphism (SNP) and insertion/deletion (INDEL) realignment, and used for marking duplicate reads, to obtain analysis-ready BAM files. The final BAM files were used as input files for variant calling. Identification of somatic mutations using the GATK Mutect2 method based on matched blood sample and population germline resource from gnomAD (*https://gnomad.broadinstitute.org/*). ANNOVAR was used to annotated variations during SNP&INDEL calling [27].

2.4. Single-cell suspension preparation

The solid tissues (including tumor and adjacent tissues) were processed to prepare single-cell suspensions. The tissue samples were cut into small pieces under aseptic conditions, and the cells were then washed twice with pre-cooled RPMI 1640 medium supplemented with 0.04% BSA. The tissues were cut into small pieces of approximately 0.5 mm^3 using surgical scissors, placed in

freshly prepared hydrolase and digested at a constant temperature of 37°C for 60 minutes, mixing every 10 minutes. The tissue was filtered 2 times using a cell sieve and centrifuged (300g) for 5 minutes at 4°C. After resuspending the sediment with an appropriate amount of medium, an equal volume of erythrocyte lysis buffer (MACS, catalog number: 130-094-183) was added. After mixing, the cells were incubated at 4°C for 10 minutes and centrifuged for 5 minutes (300g), and the number of viable cells, as determined by Trypan blue staining, was determined with a hemocytometer. Human fresh peripheral blood was collected in an anticoagulant tube and diluted with PBS at 1:1. Then, the sample was added to the Ficoll separation medium (Merck) and centrifugated 20 minutes (75g). After centrifugation, a white-grayish layer consisting of mononuclear cells will be found on top of the Ficoll-Paque. We carefully collected the mononuclear cells with a Pasteur pipette, transferred them to a new centrifuge tube, and washed them by centrifuging for 10 minutes (300g). The supernatant was discarded and resuspended in RPMI-1640 supplemented with 0.04% BSA. The number of viable cells, as determined by Trypan blue staining, was determined with a hemocytometer.

2.5. Single-cell RNA and V(D)J sequencing

The cell concentration of the freshly prepared single cell suspension was adjusted to 700-1200 cells/μl. The cDNA library amplification was performed according to the operating instructions of 10× Genomics Chromium Next GEM Single Cell 5 Reagent Kits v2.0 (PN-1000263). DNA library construction was performed using the 10x Genomics Chromium Single Cell 5' Kit (PN-1000190) following the manufacturer's guidelines. Purified cDNA libraries were sequenced using the paired-end 150 mode on an Illumina platform (Illumina NovaSeq X plus). For T-cell receptor (TCR), T cell V(D)J enrichment was performed using the 10× Genomics single cell V(D)J Enrichment Kit (TCR, PN-1000005) according to the human T cell operating instructions. The TCR library was amplified using the Chromium Single Cell TCR amplification Kit (TCR, PN-1000252), and the experimental operation was performed according to the product instructions. The constructed libraries were performed high-throughput sequencing (Illumina NovaSeq X plus) using the paired-end 150 mode at OE Biotech Co. Ltd (Shanghai, China).

2.6. scRNA-seq and scTCR-seq data processing

Raw read files were processed with Cell Ranger 7.1.0 and mapped to the GRCh38 genome assembly and counted with GRCh38 annotations. Unique molecular identifier (UMIs) was calculated by using the "cellranger count" function. As a result, a cellular gene expression matrix containing the number of gene UMIs detected in each cell was generated. In addition, we took several steps to obtain high-quality data. First, cells with high mitochondrial gene expression were removed, as dead cells often exhibit mitochondrial contamination [28]. Specifically, we followed the previous method and used the median-centered median absolute deviation (MAD)-variance normal distribution to fit the expression levels of mitochondrial genes, and removed cells with expression levels significantly higher than expected (Benjamini-Hochberg-corrected FDR < 0.01) [29]. Second, we removed cells with less than 500 or more than 6000 detected genes. Third, we used DoubletFinder [30] and scDblFinder [31] methods to identify and remove potential doublets. The 90th percentile of the doublet score of DoubletFinder was used as the cutoff value. And the expected doublet rate is 10% in scDblFinder method. Raw TCR reads were aligned to the GRCh38 reference genome and consensus TCR annotation was performed using "cellranger vdj" function (Cell Ranger 7.1.0). TCR annotation was performed using the default parameters of the 10X cellranger vdj pipeline. The R package scRepertoire was employed for clonotype assignment and dynamics analysis.

2.7. Normalization, clustering and visualization of scRNA-seq data

The gene expression matrix of the selected high-quality cells was subjected to downstream analysis using the R package Seurat (v5.0.3) [32]. The main steps include the following. First, only genes expressed in more than 5 cells were retained. Second, the raw UMI count matrix was log-normalized and scaled to 10,000 using the "LogNormalize" function. Third, 2,000 highly variable

genes were identified using the "FindVariableFeatures" function based on the normalized matrix. Fourth, the gene expression matrix was scaled and centered using the "ScaleData" function. Fifth, unsupervised clustering was performed by constructing a shared nearest neighbor (SNN) graph using the "FindNeighbors" function and the Louvain algorithm. The first 30 principal components were considered and the clustering resolution was 1.6. For uniform manifold approximation and projection (UMAP) visualization, the first two dimensions of UMAP was calculated using the "RunUMAP" function. Sixth, differential expression analysis between clusters was performed using the "FindAllMarkers" function from Seurat (using default parameters but setting min.pct to 0.5). Differential expression genes for specific clusters were identified using the "FindMarkers" function, with a threshold of $|avg\_log2FC| \geq 0.5$ and adjusted P-value ≤ 0.01. Finally, two complementary approaches are used to annotate cell clusters: (1) canonical markers; (2) markers were in the top rank of differential expressed genes.

2.8. Signature score calculation at single-cell and bulk level

Signature (module) score at single-cell level was calculated for selected gene-sets (including pathways and signatures) using "AddModuleScore_UCell" function from UCell R package. The pathways or signatures involved in this study include: immune pathways and receptors from ImmPort database (*https://immport.org/shared/home*), tissue-specific T cell signatures [33] and known cancer meta-programs [34] from previous studies, as were as several specific signatures from the molecular signatures database (MSigDB) human collections. In addition, tumor tissue upregulated and downregulated gene signatures are the top 60 up-regulated genes and the bottom 60 down-regulated genes, respectively, calculated using the TCGA-LUAD cohort. $CD8^+$ Trm and $CD4^+$ Trm signatures were identified based on "FindMarkers" function at single-cell level. Signature score at bulk level was calculated using single sample gene set enrichment analysis (ssGSEA) algorithm in R package GSVA.

2.9. Functional enrichment analysis

Differential expression analysis between malignant cells and normal cells was performed, and the up-regulated genes of malignant cells were screened according to the thresholds $avg\_log2FC \geq 0.5$ and $Padj \leq 0.01$. According to the descending sorting of avg_log2FC, the top 200 genes of malignant cells were selected. The GO BP functional enrichment analysis was performed using the R package clusterProfiler (the threshold used were $P \leq 0.001$ and $Padj \leq 0.01$). Padj calculations were based on Benjamini-Hochberg correction. The same approach was used for the comparison between the two types of malignant cells and the comparison between malignant cells in *BRCA1* and *BRCA2* mutation samples. In addition, we obtained immune signatures and gene modules of immune cell type from MSigDB hallmarks, ImmPort database, and previous studies [35, 36]. Gene set enrichment analysis (GESA) was employed to compare the immune response profile between *BRCA1* and *BRCA2* mutations using the R package enrichplot.

For all malignant cells, we performed pathway enrichment analysis using ActivePathways (v.2.0.3) R package for the terms from MSigDB (human collection C5) based on the gene sets of two meta-programs. The terms were removed once the number of genes was less than 10 or more than 500. Terms with BH-corrected significance adjusted $P \leq 0.05$ are considered to be significantly enriched by the gene sets of two meta-programs and will be retained. The significantly enrichment results were used as input to the EnrichmentMap plugin in cytoscape (v.3.9.1) software to draw a network diagram.

2.10. Single-cell copy number variation inference

The inferCNV (v.1.19.1) R package was used to distinguish malignant cells by inferring chromosomal CNVs based on the single-cell expression data. The cells from $CD8^+$ T cells as normal reference were used to estimate CNVs for the population of malignant cells. We prepared gene order files containing the chromosomal start and end positions of each gene from the GRCh38

assembly as input to the "gene_order_file" parameter in the "CreateInfercnvObject" function. To perform the infercnv operation, the count matrix and annotation file are input to create the infercnv object, and then inferCNV is run with cutoff=0.1 in the "run" function.

2.11. Identification of potential drugs targeting BRCA1-mutant genes

This study identified potential drug small molecules based on *BRCA1* mutation-related cancer-promoting factors. Gene expression profiles of lung adenocarcinoma cell lines before and after small molecule drug treatment were obtained from the NIH library of integrated network-based cellular signatures (LINCS) data resource. The connectivity Map (cMap) analysis was employed to identify potential drugs associated with molecular perturbations of four *BRCA1* mutation prognostic risk factors (4-R genes) [37]. To demonstrate the inhibitory effect of HDAC inhibitors on the growth of lung adenocarcinoma cell lines, the replication levels at different HDAC inhibitor concentrations were obtained from the cancer cell line encyclopedia (CCLE) data resource. However, due to limited data, we only obtained data on two HDAC inhibitors, entinostat and vorinostat, in 43 lung adenocarcinoma cell lines. Since drug concentrations (C) were divergent, we categorized them into 4 groups: 0 μM<C≤2 μM ([0–2]), 2 μM <C≤6 μM ([2–6]), 6 μM <C≤10 μM ([6–10]) and vehicle control (C=0 μM). The mean of each group is the average replication level of the cell line.

2.12. Cell culture and reagents

The human lung cancer cell line A549 (#SCSP-503) and the human embryonic kidney cell line HEK293T (#SCSP-502) were purchased from the Type Culture Collection of the Chinese Academy of Sciences, China. Short Tandem Repeat (STR) analyses were performed to authenticate the identity of each cell line used in this study. The A549 cells were cultured in RPMI-1640 medium (#C11875500BT; Gibco). The HEK293T cells were cultured in Dulbecco's Modified Eagle's medium (#C11995500BT; Gibco). Both cell lines were supplemented with 10% fetal bovine serum (#S712-012S; Lonsera), and grown in a humidified 5% CO_2 atmosphere at 37 °C.

2.13. Vectors and lentiviral transfection

All the short hairpin RNAs (shRNA) were cloned into the pLKO.1 vector. The target sequences are as follows:

LDHA#1: GCCACAGATTTACCCGTGGAT,
LDHA#2: GCCAACAACTTGTGTCTCAAT,
S100A10#1: TAAGGAGCCAAATACCTTGCG,
S100A10#2: CATGAAACACAAACGGCAAAT,
GAPDH#1: GTGCGGAGTGTAATCAGTATT,
GAPDH#2: TCAGGTTGTACGGGATCAAAT.

Lentiviral particles were produced by co-transfecting HEK293T cells with the shRNA plasmid and the packaging vectors psPAX2 and pMD2.G at a ratio of 4:3:1, respectively, using JetPRIME In Vitro DNA Transfection Reagent (#101000046 (114-15); Polyplus). The culture media was changed after 6 h. At 48 h post-medium change, the virus-containing medium was collected and concentrated. Viral supernatants were centrifuged at 1500 x g for 45 min, and the viral pellets were resuspended in DMEM. The lentivirus was stored at −80 °C until further use. The knockdown efficiency of the lentiviral shRNA clones was determined by western blotting.

2.14. Lentiviral infection

1×10^5 A549 cells were seeded into each well of a 6-well plate and simultaneously treated with 400 μL of lentivirus and 8 μg/mL polybrene (#28728-55-4; Selleck). The plates were incubated at 37 °C for 12 h. The cells were then passaged and seeded into new culture dishes. At 24 h post-passage, the cells infected with the lentivirus were selected with 1 μg/mL puromycin (#P8833-10mg; Sigma-Aldirch) for 3 days.

2.15. Cell proliferation assay

Cell proliferation was measured over a 4-day time course using the CellTiter-Glo® Luminescent Cell Viability Assay kit (#G9242; Promega). For this assay, 1000 cells were seeded into each well of a 96-well plate containing 100 μL of medium per well and cultured under normal conditions. At each time point, plates were cooled to room temperature, and then 100 μL of CellTiter-Glo reagent was added to each well. The contents were mixed on an orbital shaker for 2 minutes to induce cell lysis. The plate was then incubated at room temperature for 10 minutes to stabilize the luminescent signal. Finally, luminescence was measured using a microplate reader (#SLXFA-SN; Gene Company). All data were normalized to Day 1 and are presented as mean ± SD.

2.16. Drug treatment

For the cell viability assay, 5000 A549 cells were seeded into 96-well plates containing 100 μL of medium per well. After 24 h of culture at 37 °C in a 5% CO_2 atmosphere, the cells were treated with gradient concentration of the corresponding agents (Vorinostat [S1047], Belinostat [S1085], Entinostat [S1053], Pracinostat [S1515]; all from Selleck Chemicals) for 48 h. Cell viability was determined using the CellTiter-Glo® Luminescent Cell Viability Assay kit (#G9242; Promega) according to the manufacturer's instructions. To detect the protein levels of the targeted genes induced by drug treatment, 4×10^5 A549 cells were seeded into each 60-mm cell culture dish. After 24 h of culture at 37 °C in a 5% CO_2 atmosphere, the cells were treated with 1 μM and 3 μM Vorinostat or Belinostat for 2 days. The cells were then harvested to assess the protein levels of the targeted genes.

2.17. Western blotting

To assess the efficiency of lentiviral shRNA clones and the effects of drug treatments, cells were washed twice with PBS, harvested by trypsinization, and collected by centrifugation at 1500 × g for 5 min. The cell pellets were washed twice with PBS, resuspended in RIPA buffer (#P0013B; Beyotime) supplemented with a protease inhibitor cocktail (#78440; Invitrogen), incubated on ice, and then boiled for 10 min at 100°C. Protein lysates were resolved on 4-12% YoungPAGE™ Precast Gels (#PK0931; GenScript) and transferred onto a 0.45 μm Immobilon-P PVDF membrane (#IPVH00010; Merck Millipore). The membranes were blocked for 1 hr in TBST (#BL602A; Biosharp) containing 5% non-fat dry milk and subsequently incubated with primary antibodies for 1 hr at room temperature or overnight at 4°C. Following incubation with appropriate horseradish peroxidase (HRP)-conjugated secondary antibodies, signals were detected using an enhanced chemiluminescence (ECL) reagent (#CW0049M; CWBIO). Images were captured using a MiniChemi®580 + Imaging System (SINSAGE). The following antibodies were used: GAPDH Rabbit mAb (#A19056, 1:100,000; Abclonal), S100A10 Rabbit mAb (#A13634, 1:1000; Abclonal), LDHA Rabbit mAb (#A0861, 1:1000; Abclonal), β-Tubulin Rabbit mAb (#A12289, 1:10000; Abclonal), and HRP-conjugated Goat Anti-Rabbit IgG (H+L) (#111-035-003, 1:10000; Jackson).

2.18. RNA isolation and RT-qPCR

Total RNA was isolated from cells using TRIzol Reagent (#15596018; Thermo Fisher Scientific). RNA concentration was measured with a NanoDrop 2000 spectrophotometer (Thermo Fisher Scientific, USA). Total RNA was reverse transcribed into cDNA using the HiScript III 1st Strand cDNA Synthesis Kit with gDNA wiper (#R312-02; Vazyme), following the manufacturer's instructions. Quantitative reverse transcription PCR (qRT-PCR) was performed on the SLAN-96P Real-Time PCR System using ChamQ SYBR qPCR Master Mix (#Q311-02; Vazyme) and gene-specific primers according to the manufacturer's protocol. The primer sequences used for qPCR are as follows:

LDHA-fwd: 5'-ACCGTGTTATTGGAAGCGGT −3',
LDHA-rev: 5'-CTCCATGTTCCCCAAGGACC −3',
GAPDH-fwd: 5'-GTCAAGGCTGAGAACGGGAA −3',
GAPDH-rev: 5'-AAATGAGCCCCAGCCTTCTC −3',
β-actin-fwd: 5'-CACCATTGGCAATGAGCGGTTC −3',

β-actin-rev: 5'-AGGTCTTTGCGGATGTCCACGT –3'.

2.19. Statistics and survival analysis

All statistical analysis were conducted using R software (version 4.2.3, *http://www.r-project.org*). The two-sided Wilcoxon rank-sum test was employed to count and compare the differences between the two groups. Kruskal-Wallis test was used to compare the differences among the three groups. The significance level of discrete variables was calculated by Chi-squared test. The identification of prognostic factors associated with *BRCA1* and *BRCA2* mutations was based on the up-regulated genes of the corresponding mutations using univariate Cox regression analysis. Survival analysis was performed by the log-rank test and compared using Kaplan-Meier curves. Statistical significance for pairwise comparisons across the multiple groups was assessed using the Benjamini-Hochberg false discovery rate (FDR) correction. For all statistical tests, *P≤0.05; **P≤0.01; ***P≤0.001; ****P≤0.0001.

3. Results

3.1. BRCA mutations are associated with genomic instability and poor prognosis in lung adenocarcinoma

Using the TCGA-LUAD cohort data, we examined the effect of somatic mutations of *BRCA1* and *BRCA2* on genomic instability. The results showed that the mutations in both genes could significantly increase the homologous recombination repair deficiency (HRD) score and present a higher tumor mutation burden (TMB) and fraction of genome altered (FGA; Fig. 1A and Fig. S1A), indicating elevated genomic instability in LUAD tumors with *BRCA1/2* mutations. This phenomenon was also observed in *BRCA1/2* mutated patients with NSCLC (Fig. S1B-C). Furthermore, *BRCA1* and *BRCA2* mutations increased the neoantigen load in LUADs (Fig. 1A), suggesting that *BRCA1/2*-mutated tumors might be more immunogenic. By analyzing the proportion of immune subtypes [26], we found that patients with *BRCA1* mutations had a higher proportion of C1 subtype (wound healing; P=5.80e-04, Chi-squared test), while patients with *BRCA2* mutations and wild-type had a higher proportion of C3 subtype (inflammatory; P=6.61e-03, Fig. 1B). *BRCA1*-mutated patients also showed activated DNA damage repair pathways and exhibited higher DNA replication and cell cycle activity compared to wild-type patients (Fig. 1C-D), suggesting that *BRCA1* mutations may promote tumor growth through compensatory DNA repair activation—a pattern that may reflect partial HRD rather than complete loss of function.

Next, we explored the impact of *BRCA1/2* mutations on clinical outcomes of LUAD patients and found that these mutations were associated with worse prognosis for disease-free survival (DFS, P=8.46e-03, Log-rank test; Fig. 1E) and overall survival (OS, P=0.03; Fig. 1F) in multiple LUAD cohorts. In particular, *BRCA1* and *BRCA2* mutations as risk factors shortened the survival of LUAD patients (P=0.028; Fig. 1E). Interestingly, LUAD patients with BRCA mutations had significantly longer progression-free survival after ICB treatment (Fig. 1G). Through transcriptional analysis, we found that upregulation of both *BRCA1* and *BRCA2* was associated with worse prognosis after ICB treatment (P<0.05, Fig. 1H), consistent with *BRCA1/2* expression as a risk factor for lung cancers [9]. The apparent paradox between favorable ICB outcomes linked to *BRCA1/2* mutations and poorer outcomes associated with high *BRCA1/2* expression may be explained by distinct biological roles—where mutations induce genomic instability and immunogenicity, while high expression reflects proficient DNA repair and tumor cell fitness. These results suggest that BRCA abnormalities may have potential to predict ICB treatment outcomes. In addition, we found the inconsistencies in lymphocyte infiltration between *BRCA1* and *BRCA2* mutations, suggesting heterogeneity in the immune microenvironment (Fig. 1I).

3.2. Single-cell landscape of BRCA mutations in LUAD patients

Exome sequencing was performed on four samples from two individuals: two tumor tissues and two matched blood samples. The results showed that the two types of tumor tissues carried non-synonymous mutations of driver genes *TP53*, *EGFR*, and *FAT1* (Table S1), and had similar mutation

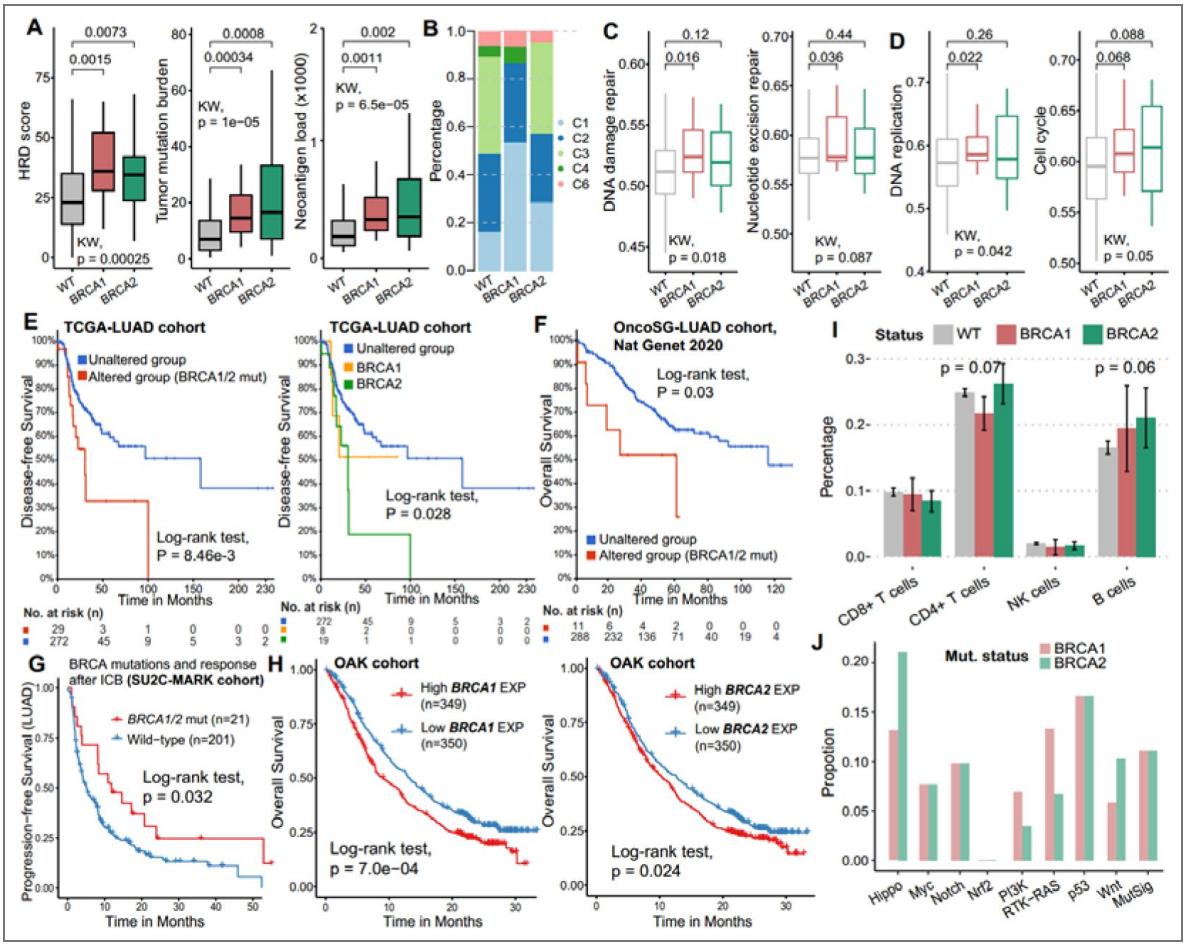

Fig. 1. *BRCA1* and *BRCA2* mutations are associated with genomic instability and poor prognosis of LUAD.

A. Distribution of HRD score, TMB and neoantigen load in patients with wild-type, *BRCA1*- and *BRCA2*- mutated lung adenocarcinoma from the TCGA-LUAD cohort (n=566). B. Proportion of immune subtypes. The significance level was calculated by Chi-squared test. C1: wound healing, C2: IFN-g dominant, C3: inflammatory, C4: lymphocyte depleted, C6: TGF-b dominant. C-D. Activity of DNA damage repair and cell cycle-related pathways in wild-type, *BRCA1*- and *BRCA2*-mutated patients (TCGA-LUAD cohort). E-F. Survival analysis of BRCA mutations in TCGA-LUAD (E) and OncoSG-LUAD (F) cohorts. G. Survival analysis of BRCA mutations in LUAD patients after ICB treatment. H. Survival analysis based on *BRCA1* (left) and *BRCA2* (right) expression in patients with ICB treatment. I. Lymphocyte infiltrates in patients with wild-type, *BRCA1* and *BRCA2* mutations (TCGA-LUAD cohort). J. Mutation frequencies of the oncogenic signaling pathway genes (in-house data).

frequencies in oncogenic signaling pathways, including p53 and Notch pathways, as well as significant mutation gene set (MutSig) scrutinized by MutSigCV [38] (Fig. 1J). Exome sequencing data show that these two types of tumor tissues harbor somatic nonsynonymous single nucleotide variants (SNV) in *BRCA2* (p.N372H) and *BRCA1* (p.E991G, p.S1566G, p.K1136R, p.P824L, and p.Y809H), respectively (Table S1). The *BRCA2* p.N372H variant lies within the BRC3 or BRC4 motifs critical for RAD51 binding. It may alter binding affinity, impair high-fidelity homologous recombination repair, and promote genomic instability [39–41]. In *BRCA1*, mutations are distributed across two key functional domains: the Coiled-Coil domain (e.g., p.E991G, p.Y809H, p.P824L) and the BRCT domain (e.g., p.K1136R, p.S1566G). Coiled-Coil mutations disrupt BRCA1-PALB2-BRCA2 complex assembly, impairing localization to DNA damage sites and subsequent *RAD51* recruitment; BRCT domain mutations compromise phospho-protein recognition and G2/M checkpoint control, leading to defective DNA damage response and unchecked proliferation of damaged cells [42–44]. Together, these defects promote the accumulation of genomic scars and chromosomal instability.

To preliminarily explore the impact of *BRCA1/2* mutations on the immune microenvironment, scRNA-seq was performed on LUAD patients carrying *BRCA1* or *BRCA2* somatic mutations (a total of 6 samples, including 2 tumors, 2 adjacent normal tissues, and 2 peripheral blood samples from one *BRCA1*-mutant and one *BRCA2*-mutant patient). A total of 69,180 high-quality cells were obtained after QC, of which 27,851 (40.3%) were from tumor tissues, 25,035 (36.2%) were from adjacent normal tissues, and 16,294 (23.5%) were from blood (Fig. 2A and Fig. S2A-B). Of these cells, 35,450 cells (51.2%) and 33,730 cells (48.8%) were from the *BRCA1*- and *BRCA2*-mutant samples, respectively. After batch correction (Harmony), we performed cell clustering and cataloged all cells into 19 main cell types annotated with canonical marker genes (Fig. 2A-C and Fig. S2A-C), identifying 4 epithelial compartments (alveolar type 1 [AT1], alveolar type 2 [AT2], ciliated, and club cells), 2 stromal compartments (fibroblasts and endothelial cells), 5 lymphocyte compartments ($CD4^+$ T, $CD8^+$ T, natural killer-NK/NKT, B cells, and plasma) and 6 myeloid compartments (macrophages, dendritic cells-DCs, classical/nonclassical monocytes, neutrophil, and mast cells). Among immune cells, the most abundant cell types were T lymphocytes and macrophages (Fig. 2B).

To distinguish malignant cells, we first inferred copy number variation (CNV) of all epithelial cell types in solid tissues using the inferCNV pipeline [45] (Fig. S2D-E). Using immune cells as a control and comparing the CNV scores of each epithelial cell subset, we identified two malignant cell subsets that were significantly clustered together using the K-means clustering algorithm and exhibited higher scores of oncogenic CNV in LUAD (Fig. 2D-E). For example, both chromosome 1q21 region and chromosome 7—frequently amplified in LUAD tumors [46, 47]—showed significantly higher CNV scores in the malignant cells of this study (Fig. 2D-E). The previously reported loss of chromosome 3q [48] was also observed in malignant cells (Fig. 2D-E). To demonstrate the properties of malignant cells, we used bulk RNA-seq data from the TCGA-LUAD cohort to identify tumor upregulated and downregulated gene signatures, and calculated module scores in different epithelial cell types. The malignant cell subsets had significantly higher tumor upregulated signature scores and lower downregulated signature scores (Fig. 2F-G and Fig. S2F). In addition, tumor marker genes, such as *CEACAM6*, *CLDN4*, and *WFDC2*, showed higher expression in malignant cells (Fig. 2H and Fig. S2C).

3.3. Distinct malignant transcriptional programs associated with *BRCA1* and *BRCA2* mutations in LUAD

We have identified two subsets of malignant cells (13,694 cells in total) from the *BRCA1/2*-mutant samples. We then asked which key molecules were specifically activated in malignant cell subsets and whether there were differences in the oncogenic programs between the *BRCA1*- and *BRCA2*-mutant cases. To address this, we first performed differential expression analysis comparing malignant cell subsets versus other epithelial cells. The results showed that tumor markers *WFDC2* and *CLDN4* were significantly upregulated in the malignant1 subset, while *CEACAM6* was significantly upregulated in both malignant cell types (Fig. S3A and Table S2). Previous studies

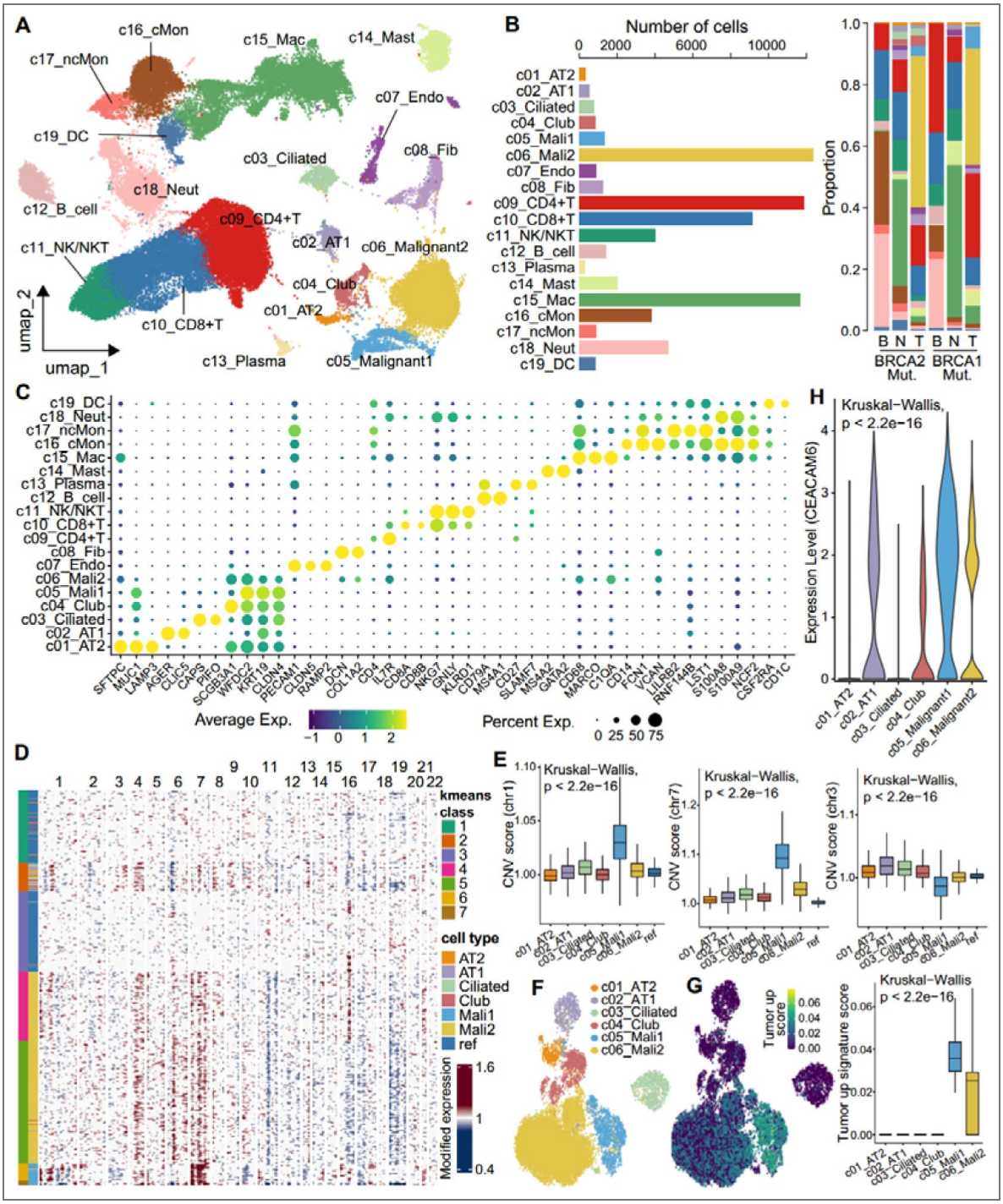

Fig. 2. Single-cell transcriptome analysis and LUAD malignant cells identification.

A. UMAP visualization of cell types in patients with *BRCA1/2* mutations (in-house data). B. The number of each cell type and its proportion in different samples, including tumor tissue (T), adjacent normal tissue (N), and peripheral blood (B). C. The bubble plot shows the expression of the markers used for cell type identification. D. The heat map inferred CNVs in epithelial cells, malignant cells, and reference cells. E. Distribution of CNV scores across different cell types on specific chromosomes. F. UMAP visualization of CNV score in epithelial cells and malignant cells. G. UMAP visualization (left) and box plot (right) of tumor upregulated signature score. H. Expression of *CEACAM6* in epithelial and malignant cells.

show that *DUSP1* could promote angiogenesis, invasion, and metastasis in NSCLC, and *FTH1* expression protects cells from cell death induced by the GPX4 inhibitor RSL3 [49, 50]. These genes upregulated in malignant cells are often also highly expressed in tumor tissues relative to paracancerous tissue (Fig. S3B). The upregulated genes in malignant1 subset were mainly enriched in ribonucleotide biosynthetic and nucleoside-related metabolic process (Fig. 3A and Table S3), suggesting enhanced DNA replication and growth abilities. In contrast, the upregulated genes of malignant2 were mainly enriched in cell adhesion, antigen processing and presentation of peptide antigen, and MHC protein complex assembly (Fig. 3A and Table S3), suggesting involvement in lymphocyte recruitment. These patterns were also observed in direct comparison between the two malignant subsets (Fig. S4A and Table S4-5).

We then applied nonnegative matrix factorization (NMF) algorithm to identify transcriptional programs consisting of co-expressed genes across all malignant cells. Using this method, we extracted a total of 4 programs and identified two meta-programs (MP1, MP2) based on program similarities (Fig. 3B). The MP1 module contains 156 genes (Table S6), whose activity was significantly higher in *BRCA2*-mutant tumor cells (Fig. 3C) and was associated with better prognosis in LUAD patients (P=0.031, Fig. 3D). The favorable prognosis linked to MP1 was related to its involvement in lymphocyte migration, T-cell chemotaxis, and myeloid leukocyte differentiation (Fig. 3E and Table S7). The MP2 module contains 200 genes involved in functions such as ATP synthesis/metabolic process and mitochondrial translation, and its activity was higher in *BRCA1*-mutant tumors (Fig. 3C, 3E, Table S6-7). To further contextualize MP1 and MP2, we obtained 41 known cancer MPs defined by Gavish et al.[34]. Among these, 15 MPs irrelevant to LUAD were excluded and 26 MPs were included. Comparing our MPs with known MPs, we found that MP1 was mainly enriched in alveolar, stress and secretion-related MPs, whereas MP2 was enriched with cell-cycle-related genes encoding HMG (high mobility group)-box proteins and with MYC-related MPs (Fig. 3F). Furthermore, *BRCA1* mutations were associated with hypoxia and oncogenic MYC-related MPs, while *BRCA2* mutations were linked to alveolar, stress and secretion-related MPs (Fig. 3G and Fig. S4B). Comparing key molecules, *BRCA1* mutation was associated with upregulation of type I IFN genes (e.g., *IFI27*, *IFITM3*), angiogenesis genes (*S100A4*, *S100A10*) and *LDHA* (Fig. 3H, Fig. S4C, and Table S8). *BRCA2* mutation was associated with upregulation of stress-related genes (e.g., *GADD45B*, *DUSP1*, and *SOD2*), immune cell-related genes (*NFKBIA*, *ICAM1*), inflammatory-related genes **(***TNFAIP3*, *CEBPB*, and *CXCL2*), and apoptosis gene *CFLAR* (Fig. 3H, Fig. S4C, and Table S8).

3.4. Inferred transcriptional trajectories from epithelial to malignant cells in *BRCA1*- and *BRCA2*-mutant tissues

Tumor evolution is a process of gradual accumulation of somatic mutations from normal cells [51]. To infer potential transcriptional transitions during malignant transformation, we analyzed the transcriptional trajectories using Monocle 2 [52], revealing a dynamic transitional spectrum from AT1/2 cells to malignant cells (Fig. 4A and Fig. S5A). The early pseudotime was dominated by AT1 and AT2 cells, primarily from tumor-adjacent and *BRCA2*-mutant tumor tissues (Fig. 4A). The trajectory then extended into two branches: one dominated by malignant1 subset (87.6% from *BRCA1*-mutant tumor), and the other almost all malignant2 subset, allowing us to explore expression gradients associated with *BRCA1* and *BRCA2* mutations (Fig. 4A). Branch fate determination gene analysis showed that the malignant1 branch upregulated genes related to oxidative phosphorylation, ATP synthesis and metabolism, and ROS response (Fig. S5B). The malignant2 branch upregulated immune-related genes such as *IL1B*, *TNFAIP3*, and *CD74*, enriched in cytokine-mediated signaling, antigen processing and presentation, and T cell activation and differentiation (Fig. S5B). This suggests heterogeneous transcriptional fates during the transition from normal lung epithelial cells to malignant cells in these two cases. We further investigated the expression differences along the inferred trajectories. The *BRCA1* mutation branch showed activation of innate immune response-related pathways such as type I IFN production, response to IFN-α/β, and upregulated genes related to T cell homeostasis/migration and T cell receptor signaling (Fig. 4B), suggesting an association with innate immune response and T cell activation.

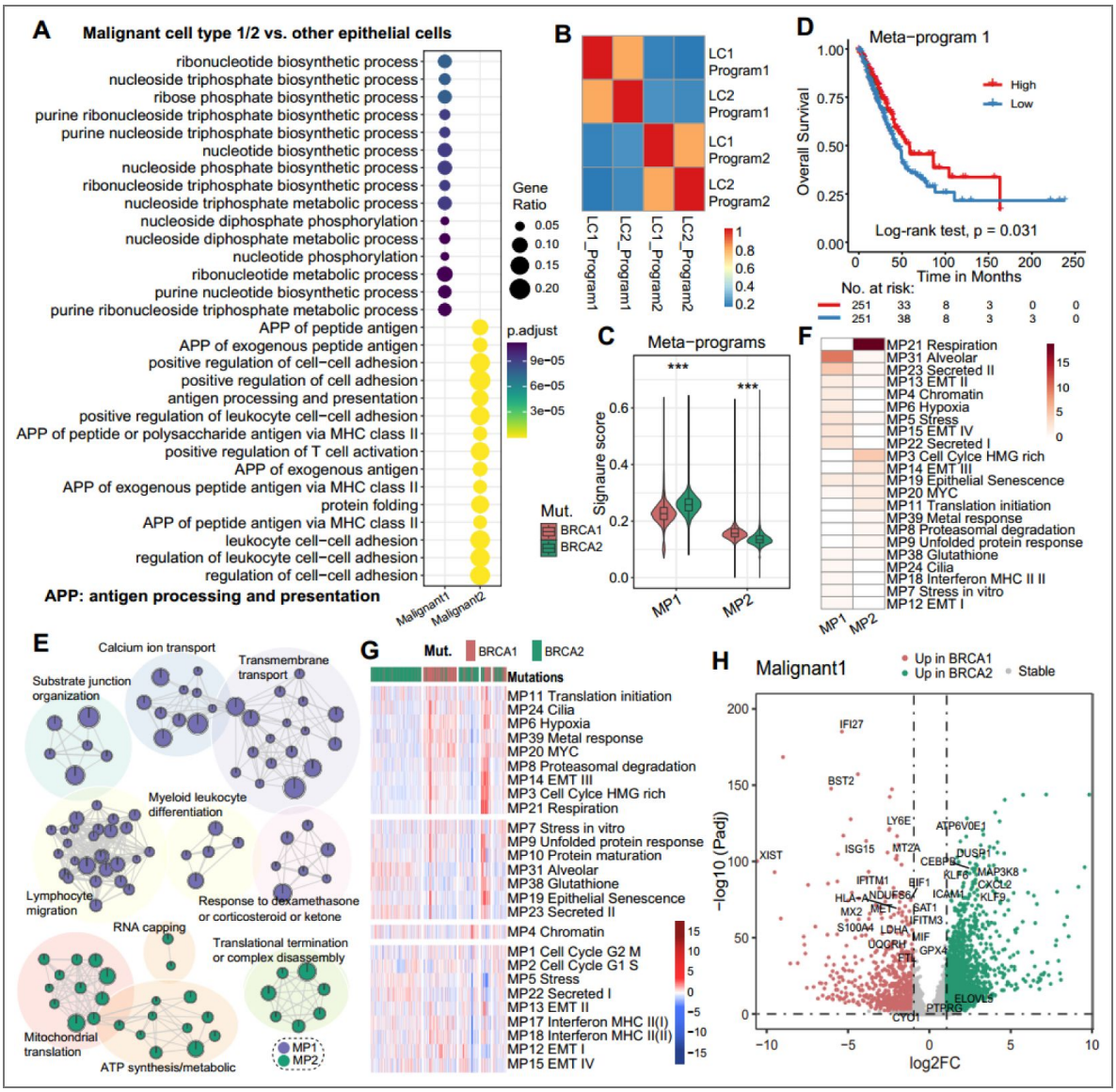

Fig. 3. Identification of key programs in *BRCA1*/2 mutated tumors.

A. Functional enrichment analysis of genes that upregulated in malignant cells relative to normal epithelial cells. B. The heat map of the similarity between pairs of programs is identified based on the NMF algorithm. C. MP score between *BRCA1* and *BRCA2* mutated malignant cells. D. K-M curves for MP1 score survival analysis. E. Enrichment map of the functions enriched by MP1 and MP2 genes. F. The overlap of in-house MPs and known cancer MPs. HMG: high mobility group. G. The heat map shows the activity of known cancer MPs in *BRCA1* and *BRCA2* mutated malignant cells. H. Volcano diagram of differentially expressed genes between *BRCA1* and *BRCA2* mutated malignant cells.

The *BRCA2* mutation branch showed activation of cell growth and development, response to wounding, and wound healing-related functions, along with promotion of MHC protein complex assembly and lymphocyte-mediated immunity (Fig. 4B), suggesting that *BRCA2* mutation may be associated with immune engagement alongside tumor growth.

Based on pseudotime order, we divided trajectories into 10 bins and analyze the activity changes of related features. The module scores of tumor downregulated genes gradually decreased along pseudotime (Fig. 4C), while tumor upregulated genes increased (Fig. S5C). Cancer MPs, such as cell cycle G2/M (MP1) and stress (MP5) increased along pseudotime in both *BRCA1*- and *BRCA2*-mutant tissues (Fig. 4D-E). Density analysis suggested that stress activation was more prominent in *BRCA2*-mutant tumor cells, while cell cycle HMG-rich program was mainly activated in the *BRCA1*-mutant group (Fig. 4F). Differences in expression programs between *BRCA1* and *BRCA2* mutations were mainly apparent in mid-to-late pseudotime. For example, *BRCA1* mutation-associated fate-determination functions such as response to IFN-α and type I IFN showed higher activity in mid-to-late pseudotime bins (Fig. 4G-H and Fig. S5D). This pattern was also observed in cGAS-STING innate immune sensing pathways, such as cGAS and IFN-γ response (Fig. 4H and Fig. S5E). In contrast, TGF-β signaling and stress modules were more active in late pseudotime in *BRCA2*-mutant cells (Fig. 4I). MHC class I and II molecules showed increased activity in late pseudotime in *BRCA1*- and *BRCA2*-mutant cells, respectively (Fig. 4G-I). This pattern was also reflected in the cell density analysis (Fig. 4J). Furthermore, $CD8^+$ Tcm and Th1 signatures exhibited higher activity in late pseudotime in *BRCA1*- and *BRCA2*-mutant cells, respectively (Fig. S5F-G). These findings suggest a differential association with $CD8^+$ versus $CD4^+$ T cell engagement.

3.5. *BRCA1* and *BRCA2* mutations reshape distinct immune microenvironment in LUAD tumors

We next explored how *BRCA1/2* mutations reshape tumor immune microenvironment of *BRCA2* mutation-upregulated genes were enriched in MHC class II-related antigen presentation and lymphocyte-mediated immunity functions (Fig. 5A). GSEA showed that MHC class II molecules were upregulated in *BRCA2* mutation group, while MHC class I molecules were upregulated in *BRCA1* mutation group (Fig. 5B-C), consistent with cell density distribution (Fig. 4J). Similarly, response to IFN-α/γ and type I IFN-related genes, as well as TNF-α family members and receptors, were enriched in *BRCA1*-mutant tumor cells (Fig. 5B-C and Fig. S6A-B). Similar patterns were observed for DNA repair, fatty acid metabolism, and $CD8^+$ T cell signatures (Fig. 5B, 5D, Fig. S6A). DNA double-strand breaks (DSBs) can lead to release of cytoplasmic dsDNA, which can be sensed by cGAS-STING signaling to trigger innate immune responses and type I IFN production, promoting anti-tumor immunity [53–55]. Based on these observations, we hypothesized that *BRCA1* mutation promote DSBs and trigger the activation of cGAS-STING signaling as well as $CD8^+$ T cell infiltration. Indeed, *BRCA1* mutations upregulated DNA damage-related checkpoints and significantly activated DSBs-related DNA repair pathways, including DNA double-strand break repair, homology-directed repair, and HRR (Fig. 5E-F and Fig. S6C-D). Furthermore, our results revealed that *BRCA1*-mutant tumors showed higher activity of cGAS-STING signaling and STING mediated induction of host immune responses compared to *BRCA2*-mutant tumors (Fig. 5G and Fig. S6F). Also, cGAS-STING signaling gens, including *cGAS*, *STING1*, and downstream factors *STAT1* and *CCL5*, were upregulated in *BRCA1*-mutant tumor cells (Fig. 5H). This observation was validated through immunofluorescence staining experiments on patient tumor tissue sections (Fig. 5I-J). Immune activity analysis suggested that *BRCA1* mutation were associated with enhanced activity of $CD8^+$ T cells and myeloid cells (Fig. S6G), consistent with GSEA results. Notably, the increased infiltration of $CD8^+$ T cells associated with *BRCA1* mutations was also confirmed in lymphocyte subsets (Fig. 5K).

Unlike *BRCA1* mutation, upregulated genes in *BRCA2*-mutant tumor cells were enriched in inflammatory response, interleukins receptor, and chemokines (Fig. 5B and Fig. S6A), which was confirmed by cell activity analysis. For example, the IL2/IL17 pathway, 4-1BB pathway, and cytokine pathway were more active in *BRCA2*-mutant tumor cells (Fig. 5E and Fig. S6C), consistent with the higher proportion of inflammatory subtypes in *BRCA2*-mutant patients (Fig.

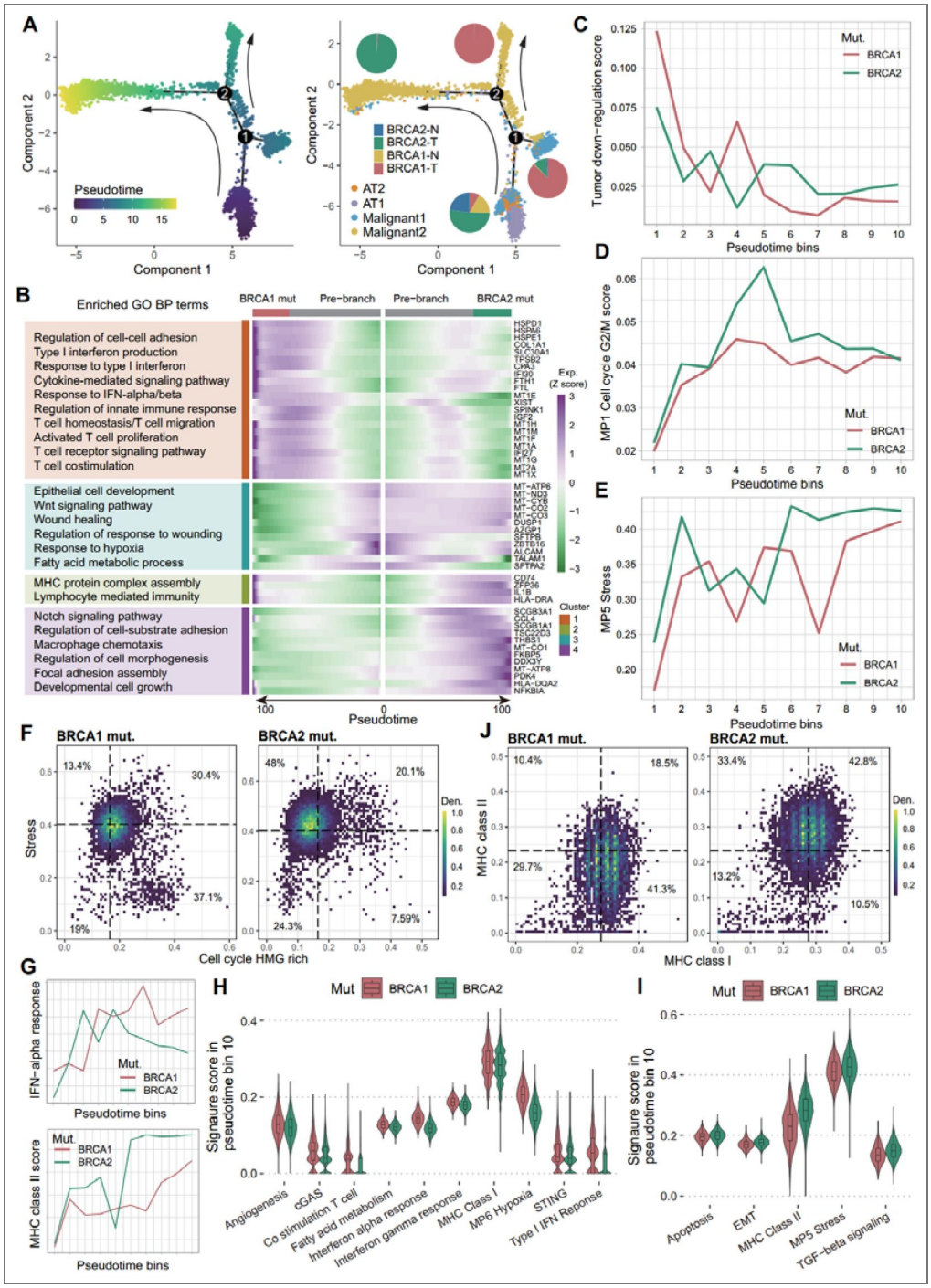

Fig. 4. Tumor evolutionary analysis of *BRCA1* and *BRCA2* mutations.

A. Pseudotime analysis of epithelial and malignant cells. The branched trajectory was colored by pseudotime (left) and cell types (right). The pie chart shows the proportion of sample groups in each branch. B. The top 50 cell fate genes and their enriched GO BP terms of *BRCA1/2* mutations in malignant2 cell type. C-E. Pseudotime was broken down into 10 bins to smooth gene expression patterns. Average gene module score between *BRCA1* and *BRCA2* mutation groups for tumor down-regulation (C), MP1 cell cycle G2/M (D), and MP5 stress (E) gene modules. F, J. Cell density distribution based on cell cycle HMG rich versus stress gene modules (F) and MHC class I versus MHC class II gene modules (J) in the same cells between *BRCA1* and *BRCA2* mutations. Color represents the density of cells. The dotted line represents the median value of the corresponding module score. G. Average gene module score for IFN-α response (top) and MHC class II (bottom) gene signatures. H-I. The activities of representative signatures between *BRCA1* and *BRCA2* mutations in bin 10 of malignant cells according to pseudotime.

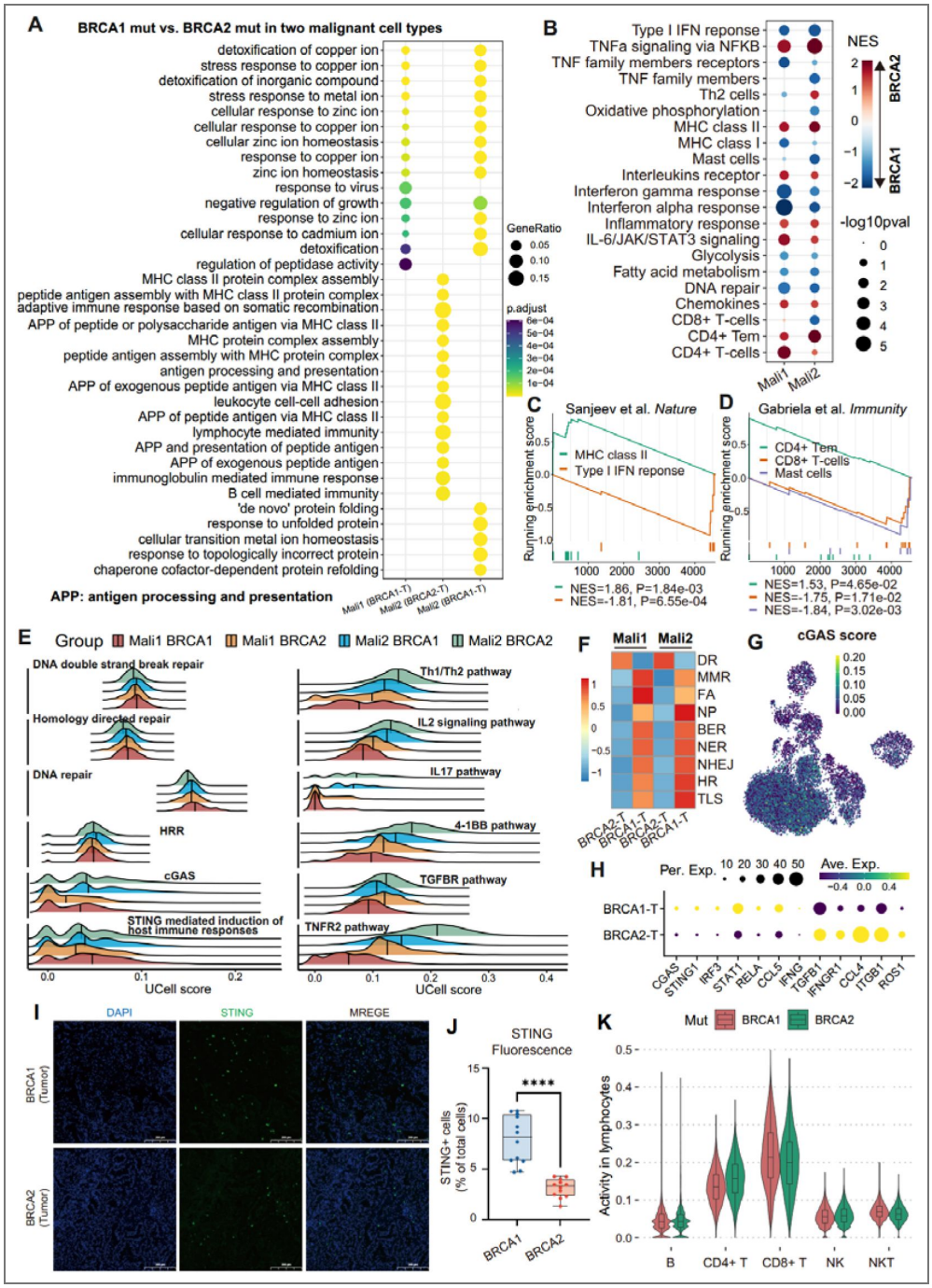

Fig. 5. *BRCA1/2* mutations are associated with tumor lymphocyte activation.

A. Functional enrichment of differentially expressed genes in malignant cells between *BRCA1* and *BRCA2* mutation groups. B. GESA of immune response profile between *BRCA1* and *BRCA2* mutations. Red (blue) indicates the gene set enriched in *BRCA2* (*BRCA1*)-mutated malignant cells. C-D. GESA plot of immune signature (C) and gene module of immune cell type (D) in malignant2 subset. NES: normalized enrichment score. E. Density ridge plot of representative pathways in two types of malignant subset with *BRCA1* and *BRCA2* mutations. HRR: homologous recombination repair. F. Mean of pathway activities related to DNA damage repair across two types of malignant cells with *BRCA1* and *BRCA2* mutations. G. UMAP visualization of cGAS pathway score. H. The expression of the representative markers. I. Immunofluorescence staining for STING (green) and DAPI (blue) on lung tumor sections from patients with *BRCA1* and *BRCA2* mutations. Scale bars, 200 μm. J. Quantification and estimation the relative intensity of the STING^{+} cells. To compare two groups, the P value was computed with the two-sided Welch's t test (ns, P>0.05; *, P<0.05; **, P<0.01; ***, P<0.001; ****, P<0.0001). K. Lymphocyte activity between *BRCA1* and *BRCA2* mutations in lymphocyte cells.

1B). In addition, *BRCA2* mutation was also associated with activation and differentiation of $CD4^+$ T cells (Fig. 5B and 5K). For example, *BRCA2*-upregulated genes were enriched in $CD4^+$ Tem signature and showed higher activity of Th1/Th2 pathways, Th1 toxicity and MHC class II modules (Fig. 5B-E and Fig. S6C). Indeed, immune activity analysis also suggested that *BRCA2*-mutant tumor cells were more associated with activation of Th1, Th2, and Treg cells compared to *BRCA1* mutations (Fig. S6G). Together, these observations suggested that *BRCA1* mutations are associated with cGAS-STING-mediated host immune responses and $CD8^+$ T cell infiltration, while *BRCA2* mutations are linked to MHC II molecule-mediated antigen presentation, inflammatory responses and $CD4^+$ T cell differentiation.

3.6. *BRCA1* and *BRCA2* mutations facilitate the clonal expansion of tissue-resident memory T cells

To examine the effect of *BRCA1/2* mutations on T lymphocytes, we obtained T cell data from BRCA wild-type in LUAD as controls from a previous study [56] and combined with our T cell data for integrated analysis. Nine T cell subsets (67,823 cells) were identified (Fig. 6A and Fig. S7A-C). Naïve T cells were mainly distributed in blood, while Teff cells were more abundant in blood and paracancerous tissues than in tumors (Fig. 6B). Treg cells were decreased in *BRCA1/2* mutant tumors compared to wild-type (Fig. S7D). We identified two tissue-resident memory T cell (Trm) subsets, $CD8^+$ Trm and $CD4^+$ Trm, both predominantly derived from tumor tissues (Fig. 6B). Interestingly, our analysis revealed that $CD8^+$ Trm cells were more abundant in *BRCA1*-mutant tumor, whereas $CD4^+$ Trm cells were more abundant in *BRCA2*-mutant tumor (Fig. 6B-D, Fig. S7D, and Fig. S8A-B). $CD8^+$ Trm cells highly expressed TNF family members and showed high activity for interferons and chemokines, similar to Teff and NK/NKT cells, whereas $CD4^+$ Trm cells upregulated chemokine receptors and cytokines receptors (Fig. S7E). Trm score of both ubsets could predict the overall survival of NSCLC patients after ICB treatment ($P<0.01$, Fig. S8C-D) and were associated with ICB response ($P<0.05$, Fig. S8E), suggesting Trm cells as potential biomarkers for ICB treatment in lung cancer.

Consistent with malignant cell results, *BRCA1* mutation was associated with upregulation of TNF family members in T lymphocytes compared to *BRCA2* mutation and wild type (Fig. S7E-G and Fig. S9). Chemokine receptor and TGF-β were more active in *BRCA2*-mutant tumor tissues (Fig. S7G-I and Fig. S9A). *BRCA1/2* mutations were associated with enhanced antigen presentation and cytokine signaling compared to wild type (Fig. S7H-J and Fig. S9A). Using tissue-specific T-cell signatures [33], we calculated activity at the single-cell level (Fig. 6E and Fig. S10A), and found that *BRCA1/2* mutations were associated with reduced CD28 family co-stimulation and decreased cytotoxic T lymphocytes (CTLs) and NKT cell infiltration compared to wild type (Fig. 6E-F), which explains why patients with *BRCA1/2* mutations showed worse prognosis (Fig. 1E-F). *BRCA1* mutations were associated with reduced TIL dysfunction and exhaustion dysfunction in tumors (Fig. 6E-F), consistent with lower expression of T cell exhaustion markers (Fig. 6G). In blood samples, *BRCA1* mutations were associated with enhanced TCR and its downstream signaling, while *BRCA2* mutations were linked to enhanced T and NK-mediated cytotoxicity and NK cell activation receptors (Fig. 6E).

Furthermore, we performed scTCR-seq to analyze the TCR clonal expansion. Teff, $CD8^+$ Trm, and $CD4^+$ Trm showed the highest hyperexpanded clonal types (Fig. 6H-I and Fig. S10B-C), suggesting antigen-driven activation. *BRCA1*-mutant samples had a higher proportion of expanded TCR clonotypes compared to *BRCA2*, across sample types (Fig. 6J and Fig. S10D). In addition, *BRCA1* mutations were associated with higher TCR diversity in tumor and blood, while *BRCA2* mutations increased TCR richness in blood (Fig. S10E). In *BRCA1*-mutant patient, shared clonotypes tended to expand in paracancerous tissue and were more shared between blood and tumor tissues (Fig. 6K and Fig. S10F-G). However, in *BRCA2*-mutant patient, shared clonotypes tended to expand in blood and paracancerous tissue (Fig. 6K and Fig. S10F). *BRCA1* mutations were associated expansion of Teff, $CD8^+$ Trm, and Tem in solid tissues, while $CD4^+$ Trm expansion was more prominent in *BRCA2* mutations (Fig. 6L and Fig. S10H). This was especially evident among the top 50 expanded TCR clonotypes (Fig. 6M). Teff was the most expansion subset in blood,

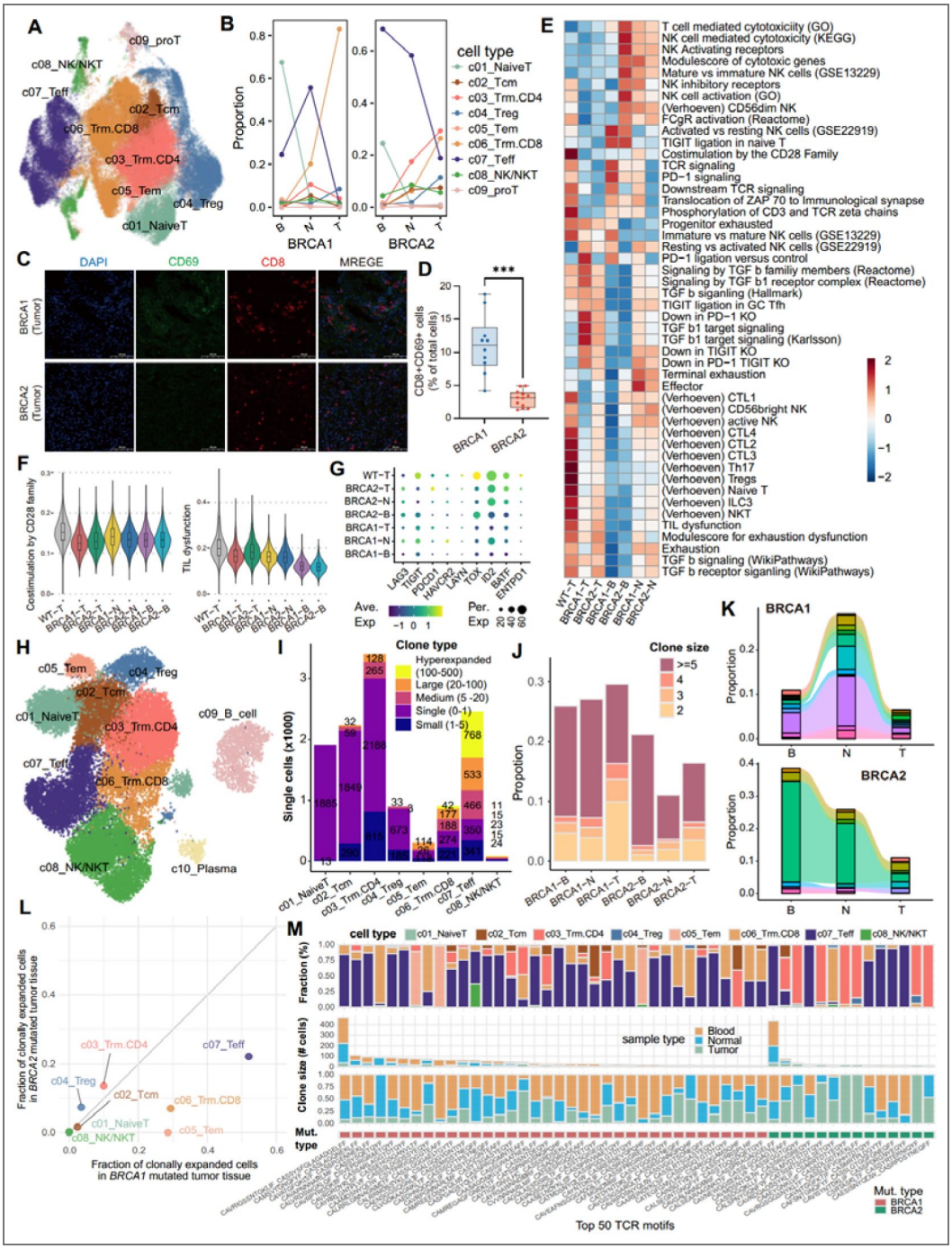

Fig. 6. T lymphocyte infiltration and TCR clonal expansion analysis.

A-B. UMAP visualization (A) and proportion (B) of T lymphocyte subsets in combined dataset. C. Multiplex immunofluorescence staining for CD8 (red), CD69 (green), and DAPI (blue) on lung tumor sections from patients with *BRCA1* and *BRCA2* mutations. Scale bars, 100 μm. D. Quantification the relative intensity of the $CD8^+$ $CD69^+$ cells. The P value was computed with the two-sided Welch's t test (ns, P>0.05; *, P<0.05; **, P<0.01; ***, P<0.001). E-F. The activity of tissue-specific T cell signatures from Judith Wienke et al. G. Terminal exhaustion marker expression levels. H. UMAP of lymphocyte subsets in in-house dataset. I. Quantification of clonal size across sample types. Clonotypes are ranked by expansion level, including: single (1 cell), small (>1 and <5 cells), medium (>5 and <20 cells), large (>20 and <100 cells), and hyperexpanded (>100 and <500 cells). J. Expanded clonotypes distribution in different samples. K. Proportional and dynamic changes in shared clonotypes (top5 per group) between different samples within the same patient. The colors represent different clonotypes. L. The proportion of clonally expanded cells (≥5 clone size) in *BRCA1/2* mutated tumor tissues for specific cell types. M. The sample and cell proportions of the 50 most abundant TCR motifs.

regardless of mutation type (Fig. 6M and Fig. S10I). Together, these results suggest that *BRCA1* mutations are associated with increase antigen exposure and $CD8^+$ Trm expansion, while *BRCA2* mutations are linked to $CD4^+$ Trm expansion in tumor tissue and enhanced T/NK toxicity in blood.

3.7. Targeting a *BRCA1* mutation-associated transcriptional program inhibits LUAD tumor growth in vitro

Our analyses suggested that *BRCA1/2* mutations are associated with distinct transcriptional programs. Then, we identified BRCA mutation-related prognostic factors using Cox regression analysis. The results showed that the factors associated with *BRCA2* mutation were linked to longer patient survival (HR<1, Table S9), and a *BRCA2* signature score predicted better survival (P=0.0015, Fig. S11A), consistent with upregulation of MHC complex assembly genes. After receiving ICB treatment, lung cancer patients with high *BRCA2* signature scores show longer survival and better responses (P<0.0001; Fig. S11B-C and Fig. S12A). In contrast, a *BRCA1* mutation prognostic factor was associated with shorter survival (HR>1, Table S9), and its signature score predicted worse survival in patients with LUAD (P=0.0012; Fig. 7A and Fig. S12B) and NSCLC (P=0.0013; Fig. 7B, suggesting that *BRCA1* mutation activates a tumor-promoting program. Based on this, we identified four *BRCA1* mutation-associated risk genes (*S100A10*, *LDHA*, *MYL12A*, and *GAPDH*; termed the 4-R genes) for subsequent analysis, which were associated with worse overall survival (Fig. 7C and Fig. S11F). Immunofluorescence experiments on patient tissue sections revealed that *S100A10* was upregulated in *BRCA1*-mutated tumor tissue relative to adjacent non-cancerous tissue (Fig. S11D-E). Previous studies have shown that *S100A10* can promote cancer metastasis by recruiting MDSC cells, and increased *LDHA* activity contributes to tumor immune escape [57, 58]. In our study, knockdown of *S100A10*, *LDHA*, and *GAPDH* reduced LUAD cell proliferation *in vitro* (Fig. 7D-E).

We next asked whether small molecules could reduce the expression of these risk genes and inhibit LUAD growth. Using gene expression profiles of A549 cells before and after drug treatment from LINCS data resource, we performed cMap analysis to identify drugs that perturb 4-R gene expression. Interestingly, histone deacetylase (HDAC) inhibitors consistently downregulated 4-R genes in A549 cells (Fig. 7F and Table S10). Cell growth decreased significantly with increasing HDAC inhibitor concentrations (Fig. 7 G-H, Fig. S11G-H, and Table S11). Vorinostat (FDA-approved for cutaneous T cell lymphoma) significantly inhibited 4-R gene expression (NCS<-1, P<0.01; Fig. 7F and Table S10). Furthermore, vorinostat and belinostat reduced expression of *LDHA*, *S100A10*, and *GAPDH* in A549 cells in a dose-dependent manner (Fig. 7I-J and Fig. S11I). Other HDAC inhibitors (mocetinostat, entinostat, and SB-939) also showed similar effects on the perturbation of 4-R genes (Fig. 7F-H and Table S10). These findings suggested that HDAC inhibitors may target *BRCA1* mutation-associated risk genes and inhibit LUAD tumor growth *in vitro*, offering a preliminary therapeutic hypothesis for further testing.

4. Discussion

Our study provides a comprehensive molecular and cellular characterization of the TME in LUAD with *BRCA1* and *BRCA2* mutations, using large-scale multi-omics data and single-cell data. We describe transcriptional and immune patterns associated with these mutations, which may contribute to genomic instability, immune cell infiltration, and immune modulation within the TME. These observations offer hypotheses for understanding HRR deficiency in LUAD and for developing potential therapeutic strategies, including ICB and targeted therapies. HRR deficiency is a key contributor to tumorigenesis and treatment response in multiple cancers [7]. Although HRR deficiency has been correlated with enhanced sensitivity to DNA-damaging agents and ICB in cancers such as breast, ovarian, and NSCLC, our study suggests that in LUAD, *BRCA1/2* mutations may be associated with distinct TME features that could influence immunotherapy effectiveness. This underscores the complexity of BRCA-driven biology in LUAD.

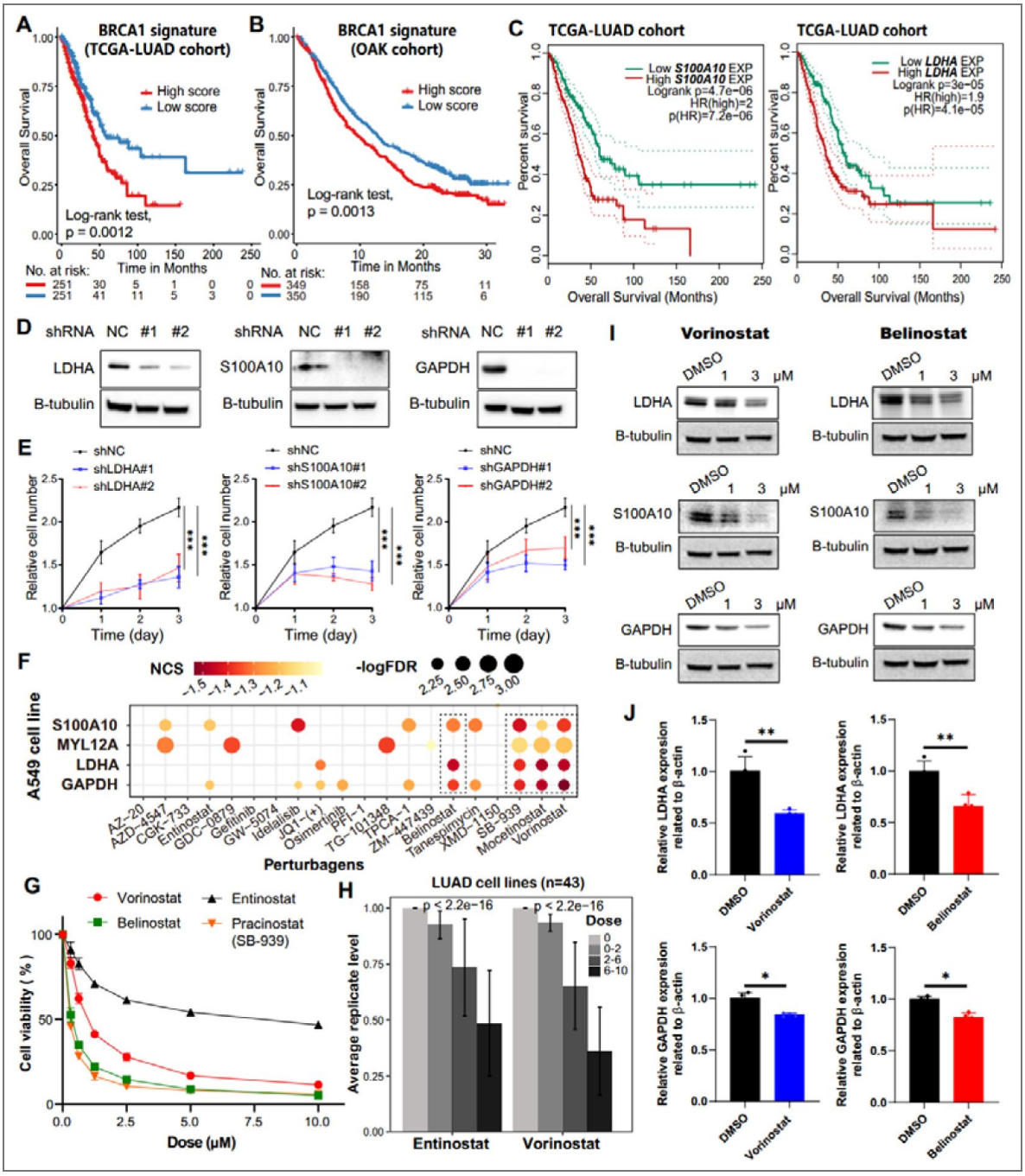

Fig. 7. Targeting *BRCA1* mutation-related risk genes inhibits tumor growth.

A-B. Survival analysis of *BRCA1*-mutant signature score in TCGA-LUAD (A) and OAK (B) cohorts. C. Survival analysis of *S100A10* (left) and *LDHA* (right) in TCGA-LUAD cohort according to the expression median. D. The effects of sh-*LDHA*, *S100A10*, and *GAPDH* on protein levels in A549 cell line (The original image is shown in Fig. S13A). E. The effects of sh-*LDHA*, *S100A10*, *GAPDH*, and vector on cell proliferation were determined by a cell proliferation assay in A549 LUAD cell line. F. The molecular perturbations of 4-R genes in A549 cell line at 10 μM concentration (24 h) from the LINCS data resource. NCS: Normalized connectivity score. G. The effects of HDAC inhibitors concentration on cell proliferation in A549 cell line. H. Cell replication levels after treatment with different concentrations of entinostat (left) and vorinostat (right) in LUAD cell lines. I. The protein levels of *LDHA*, *S100A10*, and *GAPDH* after treatment with vorinostat (left) and belinostat (right) in A549 cell line were measured using western blotting (The original image is shown in Fig. S13B). J. The mRNA levels of *LDHA* and *GAPDH* after treatment (3 μM) with vorinostat (left) and belinostat (right) in A549 cell line were measured using qPCR. Significance levels were determined by Student's t-test. For all statistical tests, *P≤0.05; **P≤0.01; ***P≤0.001.

A key aspect of this study is the single-cell transcriptomic profiling of *BRCA1/2*-mutant LUAD tumors, paracancerous tissues, and peripheral blood patients. This enabled high-resolution examination of immune signatures, though the sample size limits generalizability. *BRCA1* mutations were associated with the upregulation of cGAS-STING and type I IFN response gene, which can enhance innate immune responses, antigen presentation, and cytotoxic T-cell activity [59]. *BRCA1*-mutant tumors showed higher $CD8^+$ T cell activation and MHC-I expression, possibly due to increased neoantigen load. This suggests that *BRCA1*-mutant tumors may be more immunogenic and potentially responsive to immunotherapy. In contrast, *BRCA2* mutation was associated with upregulated MHC-II expression, which plays a role in antigen presentation and $CD4^+$ T cell recruitment [60], suggesting a shift toward adaptive immunity and antigen-presenting cell involvement. *BRCA2*-mutant tumors showed higher $CD4^+$ T cell activation, particularly inflammatory subsets, and were associated with increased NK cell activity and T cell cytotoxicity in blood, suggesting systemic immune engagement.

Despite these immune signatures, *BRCA1/2* mutations were associated with downregulation of CD28 family co-stimulatory molecules, essential for effective T cell activation [61]. This may indicate adaptive resistance mechanisms. ICB may overcome such resistance (e.g., blocking PD-L1), unleashing the pre-existing, infiltration-potentiated immune response (Fig. 1G). We identified two Trm subsets ($CD8^+$ Trm and $CD4^+$ Trm) as potential biomarkers for ICB response in NSCLC. *BRCA1* mutation was associated with $CD8^+$ Trm TCR expansion, while *BRCA2* mutation was linked to $CD4^+$ Trm expansion, which may contribute to maintain a chronic inflammatory TME [62, 63]. Given the observed T cell infiltration and IFN-driven immune activation, *BRCA1*-mutant tumors might initially respond well to anti-PD-1/PD-L1 therapies. However, *BRCA1* mutations also activated risk genes (*S100A10*, *LDHA*, *GAPDH*, and *MYL12A*). We identified HDAC inhibitors as potential agents targeting this program. HDAC inhibitors can modulate chromatin accessibility, reduce immune suppression, and enhance tumor immunogenicity, suggesting that combining them with ICB might enhance immune response and overcome resistance mechanisms in *BRCA1*-driven tumors.

Despite the comprehensive multi-omics and single-cell analyses conducted in this study, several limitations should be acknowledged. Although we included both tumor tissues and matched paracancerous and blood samples, the sample size remains modest, which may limit the statistical power and generalizability of our findings. Therefore, our results should be interpreted as preliminary, and further studies with larger, independent cohorts are required to validate these observations. Single-cell RNA-seq and TCR-seq analyses in this study provide high-resolution insights into the cellular and clonal dynamics of the TME, the functional validation of key mechanisms remains largely correlative. While our *in vitro* experiments provide valuable mechanistic insight, the lack of *in vivo* validation, which cannot fully recapitulate the complex TME. Future studies utilizing murine models or patient-derived organoids are essential to establish causal relationships and elucidate the underlying molecular pathways. The efficacy and safety of combining HDAC inhibitors with ICB in *BRCA1*-mutant LUAD patients remain unexplored and represent an important avenue for future research.

5. Conclusions

Overall, this study provides a high-resolution molecular map of the TME in *BRCA1/2*-mutant LUAD, highlighting distinct immune and transcriptional signatures associated with each mutation in the profiled cases. By uncovering these molecular distinctions, our study offers a hypothesis-generating framework for understanding HRR deficiency in LUAD and lays groundwork for future validation and precision immunotherapy strategies tailored to *BRCA1/2* mutation status.

Data availability

The raw data of single-cell sequencing (including scRNA-seq and scTCR-seq) and the processed data generated in this study have been deposited at the Gene Expression Omnibus (GEO) repository, with the accession code GSE292700. Open-source R packages and software, as well as

standard workflows were used in this study. No previously unreported custom code was developed for the analyses presented. All codes and other processed data are available from the corresponding author upon reasonable request.

Acknowledgements

The authors wish to thank the staff members from Affiliated Cancer Hospital and Institute of Guangzhou Medical University. High-throughput sequencing was performed by the OE Biotech Co., Ltd. (Shanghai, China). The contribution of the bioinformatics core facility at Guangzhou medical university is gratefully acknowledged.

Additional information

CRediT authorship contribution statement

Gaoming Liao: Writing - original draft, Visualization, Formal analysis, Data curation, Conceptualization, Software, Methodology, Funding acquisition. **Xinbin Yang**: Writing - review & editing, Investigation, Methodology. **Qi Liu**: Writing - review & editing, Investigation, Validation. **Shufeng Nan**: Validation, Software. **Yan Liu**: Software. **Jinwei Li**: Validation. **Si Huang**: Validation. **Wang Ning**: Validation. **Xionghai Qin**: Writing - review & editing, Supervision, Conceptualization. **Gang Xu**: Writing - review & editing, Project administration, Supervision, Conceptualization.

Funding

This study was supported by the National Natural Science Foundation of China (Grant No. 82403816), the China Postdoctoral Foundation (Grant No. 2023M740846), the Guangdong Basic and Applied Basic Research Foundation (Grant No. 2023A1515110297), the Beijing Vlove Charity Foundation (Grant No. RXYS2025-0100630114), and the Fundamental Research Funds for the Provincial Universities (Grant No. 2023-KYYWF-0212).

Abbreviations

NSCLC: Non-small cell lung cancer
LUAD: Lung adenocarcinoma
HRR: Homologous recombination repair
HRD: Homologous recombination repair deficiency
TMB: Tumor mutation burden
TME: Tumor microenvironment
ICB: Immune checkpoint blockade
Trm: Tissue-resident memory T cell
HDAC: Histone deacetylase
BRCA1/2: BReast CAncer gene 1/2
TCGA: The cancer genome atlas
UMI: Unique molecular identifier
UMAP: Uniform manifold approximation and projection
TCR: T-cell receptor
MSigDB: Molecular signatures database
ssGSEA: Single sample gene set enrichment analysis
NMF: Nonnegative matrix factorization
cMap: Connectivity Map
LINCS: Library of integrated network-based cellular signatures
CCLE: Cancer cell line encyclopedia

Funding

Funder	Grant reference number	Author
MOST | National Natural Science Foundation of China (NSFC)	82403816	Gaoming Liao
China Postdoctoral Science Foundation (中国博士后科学基金会职)	2023M740846	Gaoming Liao
Fundamental Research Funds for the Provincial Universities	2023-KYYWF-0212	Xionghai Qin
Beijing Vlove Charity Foundation	RXYS2025-0100630114	Gang Xu
Guangdong Basic and Applied Basic Research Foundation	2023A1515110297	Gaoming Liao

Author ORCID iDs

Gaoming Liao: https://orcid.org/0009-0005-6414-3670

Additional files

Supplementary Figures 1–12.

Supplementary Figure 13.

Supplementary Tables 1–11.

References

[1] **Myers D.J.,** Wallen J.M. (2025) *Lung Adenocarcinoma* StatPearls.

[2] **Skoulidis F.,** Heymach J.V. (2019) Co-occurring genomic alterations in non-small-cell lung cancer biology and therapy. *Nat Rev Cancer* **19**:495-509 https://doi.org/10.1038/s41568-019-0179-8 | PubMed

[3] **Nguyen B.,** Fong C., Luthra A., Smith S.A., DiNatale R.G., Nandakumar S., Walch H., Chatila W.K., Madupuri R., Kundra R., *et al.* (2022) Genomic characterization of metastatic patterns from prospective clinical sequencing of 25,000 patients. *Cell* **185**:563-575. https://doi.org/10.1016/j.cell.2022.01.003 | PubMed

[4] **Novikov N.M.,** Zolotaryova S.Y., Gautreau A.M., Denisov E.V. (2021) Mutational drivers of cancer cell migration and invasion. *Br J Cancer* **124**:102-114 https://doi.org/10.1038/s41416-020-01149-0 | PubMed

[5] **de Visser K.E.,** Joyce J.A. (2023) The evolving tumor microenvironment: From cancer initiation to metastatic outgrowth. *Cancer Cell* **41**:374-403 https://doi.org/10.1016/j.ccell.2023.02.016 | PubMed

[6] **Giraldo N.A.,** Sanchez-Salas R., Peske J.D., Vano Y., Becht E., Petitprez F., Validire P., Ingels A., Cathelineau X., Fridman W.H., *et al.* (2019) The clinical role of the TME in solid cancer. *Br J Cancer* **120**:45-53 https://doi.org/10.1038/s41416-018-0327-z | PubMed

[7] **Hoppe M.M.,** Sundar R., Tan D.S.P., Jeyasekharan A.D. (2018) Biomarkers for Homologous Recombination Deficiency in Cancer. *J Natl Cancer Inst* **110**:704-713 https://doi.org/10.1093/jnci/djy085 | PubMed

[8] **Liao G.,** Jiang Z., Yang Y., Zhang C., Jiang M., Zhu J., Xu L., Xie A., Yan M., Zhang Y., *et al.* (2021) Combined homologous recombination repair deficiency and immune activation analysis for predicting intensified responses of anthracycline, cyclophosphamide and taxane chemotherapy in triple-negative breast cancer. *BMC Med* **19**:190 https://doi.org/10.1186/s12916-021-02068-4 | PubMed

[9] **Yan B.,** Xie B., Huang M., Guo J., Sun J., Chen J., Tao Y., Xiao D. (2023) Mutations and expressions of breast cancer 1/2 in lung cancer. *Thorac Cancer* **14**:1753-1763 https://doi.org/10.1111/1759-7714.14920 | PubMed

[10] **Samstein R.M.,** Krishna C., Ma X., Pei X., Lee K.W., Makarov V., Kuo F., Chung J., Srivastava R.M., Purohit T.A., *et al.* (2021) Mutations in BRCA1 and BRCA2 differentially affect the tumor microenvironment and response to checkpoint blockade immunotherapy. *Nat Cancer* **1**:1188-1203 https://doi.org/10.1038/s43018-020-00139-8 | PubMed

[11] **Bruand M.,** Barras D., Mina M., Ghisoni E., Morotti M., Lanitis E., Fahr N., Desbuisson M., Grimm A., Zhang H., *et al.* (2021) Cell-autonomous inflammation of BRCA1-deficient ovarian cancers drives both tumor-intrinsic immunoreactivity and immune resistance via STING. *Cell Rep* **36**:109412 https://doi.org/10.1016/j.celrep.2021.109412 | PubMed

[12] **Francis J.C.,** Melchor L., Campbell J., Kendrick H., Wei W., Armisen-Garrido J., Assiotis I., Chen L., Kozarewa I., Fenwick K., *et al.* (2015) Whole-exome DNA sequence analysis of Brca2- and Trp53-deficient mouse mammary gland tumours. *J Pathol* **236**:186-200 https://doi.org/10.1002/path.4517 | PubMed

[13] **Lee Y.C.,** Lee Y.C., Li C.Y., Lee Y.L., Chen B.L. (2020) BRCA1 and BRCA2 Gene Mutations and Lung Cancer Sisk: A Meta-Analysis. *Medicina (Kaunas)* **56** https://doi.org/10.3390/medicina56050212 | PubMed

[14] **Chabanon R.M.,** Pedrero M., Lefebvre C., Marabelle A., Soria J.C., Postel-Vinay S. (2016) Mutational Landscape and Sensitivity to Immune Checkpoint Blockers. *Clin Cancer Res* **22**:4309-21 https://doi.org/10.1158/1078-0432.ccr-16-0903 | PubMed

[15] **Zhou Z.,** Ding Z., Yuan J., Shen S., Jian H., Tan Q., Yang Y., Chen Z., Luo Q., Cheng X., *et al.* (2022) Homologous recombination deficiency (HRD) can predict the therapeutic outcomes of immuno-neoadjuvant therapy in NSCLC patients. *J Hematol Oncol* **15**:62 https://doi.org/10.1186/s13045-022-01283-7 | PubMed

[16] **Papadaki C.,** Sfakianaki M., Ioannidis G., Lagoudaki E., Trypaki M., Tryfonidis K., Mavroudis D., Stathopoulos E., Georgoulias V., Souglakos J. (2012) ERCC1 and BRAC1 mRNA expression levels in the primary tumor could predict the effectiveness of the second-line cisplatin-based chemotherapy in pretreated patients with metastatic non-small cell lung cancer. *J Thorac Oncol* **7**:663-71 https://doi.org/10.1097/jto.0b013e318244bdd4 | PubMed

[17] **Bonanno L.,** Costa C., Majem M., Favaretto A., Rugge M., Rosell R. (2013) The predictive value of BRCA1 and RAP80 mRNA expression in advanced non-small-cell lung cancer patients treated with platinum-based chemotherapy. *Ann Oncol* **24**:1130-2 https://doi.org/10.1093/annonc/mdt063 | PubMed

[18] **Motohashi T.,** Isobe K., Yoshizawa T., Usui Y., Shimizu H., Sekiya M., Miyoshi S., Nakamura Y., Urabe N., Sakamoto S., *et al.* (2024) BRCA2-positive lung adenocarcinoma treated with olaparib: A case report. *Respirol Case Rep* **12**:e01317 https://doi.org/10.1002/rcr2.1317 | PubMed

[19] **Jovic D.,** Liang X., Zeng H., Lin L., Xu F., Luo Y. (2022) Single-cell RNA sequencing technologies and applications: A brief overview. *Clin Transl Med* **12**:e694 https://doi.org/10.1002/ctm2.694 | PubMed

[20] **Travaglini K.J.,** Nabhan A.N., Penland L., Sinha R., Gillich A., Sit R.V., Chang S., Conley S.D., Mori Y., Seita J., *et al.* (2020) A molecular cell atlas of the human lung from single-cell RNA sequencing. *Nature* **587**:619-625 https://doi.org/10.1038/s41586-020-2922-4 | PubMed

[21] **Haque A.,** Engel J., Teichmann S.A., Lonnberg T. (2017) A practical guide to single-cell RNA-sequencing for biomedical research and clinical applications. *Genome Med* **9**:75 https://doi.org/10.1186/s13073-017-0467-4 | PubMed

[22] **Frank M.L.,** Lu K., Erdogan C., Han Y., Hu J., Wang T., Heymach J.V., Zhang J., Reuben A. (2023) T-Cell Receptor Repertoire Sequencing in the Era of Cancer Immunotherapy. *Clin Cancer Res* **29**:994-1008 https://doi.org/10.1158/1078-0432.ccr-22-2469 | PubMed

[23] **Chen J.,** Yang H., Teo A.S.M., Amer L.B., Sherbaf F.G., Tan C.Q., Alvarez J.J.S., Lu B., Lim J.Q., Takano A., *et al.* (2020) Genomic landscape of lung adenocarcinoma in East Asians. *Nat Genet* **52**:177-186 https://doi.org/10.1038/s41588-019-0569-6 | PubMed

[24] **Ravi A.,** Hellmann M.D., Arniella M.B., Holton M., Freeman S.S., Naranbhai V., Stewart C., Leshchiner I., Kim J., Akiyama Y., *et al.* (2023) Genomic and transcriptomic analysis of checkpoint blockade response in advanced non-small cell lung cancer. *Nat Genet* **55**:807-819 https://doi.org/10.1038/s41588-023-01355-5 | PubMed

[25] **Patil N.S.,** Nabet B.Y., Muller S., Koeppen H., Zou W., Giltnane J., Au-Yeung A., Srivats S., Cheng J.H., Takahashi C., *et al.* (2022) Intratumoral plasma cells predict outcomes to PD-L1 blockade in non-small cell lung cancer. *Cancer Cell* **40**:289-300. https://doi.org/10.1016/j.ccell.2022.02.002 | PubMed

[26] **Thorsson V.,** Gibbs D.L., Brown S.D., Wolf D., Bortone D.S., Ou Yang T.H., Porta-Pardo E., Gao G.F., Plaisier C.L., Eddy J.A., *et al.* (2018) The Immune Landscape of Cancer. *Immunity* **48**:812-830. https://doi.org/10.1016/j.immuni.2018.03.023 | PubMed

[27] **Wang K.,** Li M., Hakonarson H. (2010) ANNOVAR: functional annotation of genetic variants from high-throughput sequencing data. *Nucleic Acids Res* **38**:e164 https://doi.org/10.1093/nar/gkq603 | PubMed

[28] **Ilicic T.,** Kim J.K., Kolodziejczyk A.A., Bagger F.O., McCarthy D.J., Marioni J.C., Teichmann S.A. (2016) Classification of low quality cells from single-cell RNA-seq data. *Genome Biol* **17**:29 https://doi.org/10.1186/s13059-016-0888-1 | PubMed

[29] **Pijuan-Sala B.,** Griffiths J.A., Guibentif C., Hiscock T.W., Jawaid W., Calero-Nieto F.J., Mulas C., Ibarra-Soria X., Tyser R.C.V., Ho D.L.L., *et al.* (2019) A single-cell molecular map of mouse gastrulation and early organogenesis. *Nature* **566**:490-495 https://doi.org/10.1038/s41586-019-0933-9 | PubMed

[30] **McGinnis C.S.,** Murrow L.M., Gartner Z.J. (2019) DoubletFinder: Doublet Detection in Single-Cell RNA Sequencing Data Using Artificial Nearest Neighbors. *Cell Syst* **8**:329-337. https://doi.org/10.1016/j.cels.2019.03.003 | PubMed

[31] **Germain P.L.,** Lun A., Garcia Meixide C., Macnair W., Robinson M.D. (2021) Doublet identification in single-cell sequencing data using scDblFinder. *F1000Res* **10**:979 https://doi.org/10.12688/f1000research.73600.2 | PubMed

[32] **Hao Y.,** Stuart T., Kowalski M.H., Choudhary S., Hoffman P., Hartman A., Srivastava A., Molla G., Madad S., Fernandez-Granda C., *et al.* (2024) Dictionary learning for integrative, multimodal and scalable single-cell analysis. *Nat Biotechnol* **42**:293-304 https://doi.org/10.1038/s41587-023-01767-y | PubMed

[33] **Wienke J.,** Visser L.L., Kholosy W.M., Keller K.M., Barisa M., Poon E., Munnings-Tomes S., Himsworth C., Calton E., Rodriguez A., *et al.* (2024) Integrative analysis of neuroblastoma by single-cell RNA sequencing identifies the NECTIN2-TIGIT axis as a target for immunotherapy. *Cancer Cell* **42**:283-300. https://doi.org/10.1016/j.ccell.2023.12.008 | PubMed

[34] **Gavish A.,** Tyler M., Greenwald A.C., Hoefflin R., Simkin D., Tschernichovsky R., Galili Darnell N., Somech E., Barbolin C., Antman T., *et al.* (2023) Hallmarks of transcriptional intratumour heterogeneity across a thousand tumours. *Nature* **618**:598-606 https://doi.org/10.1038/s41586-023-06130-4 | PubMed

[35] **Mariathasan S.,** Turley S.J., Nickles D., Castiglioni A., Yuen K., Wang Y., Kadel E.E., Koeppen H., Astarita J.L., Cubas R., *et al.* (2018) TGFbeta attenuates tumour response to PD-L1 blockade by contributing to exclusion of T cells. *Nature* **554**:544-548 https://doi.org/10.1038/nature25501 | PubMed

[36] **Bindea G.,** Mlecnik B., Tosolini M., Kirilovsky A., Waldner M., Obenauf A.C., Angell H., Fredriksen T., Lafontaine L., Berger A., *et al.* (2013) Spatiotemporal dynamics of intratumoral immune cells reveal the immune landscape in human cancer. *Immunity* **39**:782-95 https://doi.org/10.1016/j.immuni.2013.10.003 | PubMed

[37] **Liao G.,** Yang Y., Xie A., Jiang Z., Liao J., Yan M., Zhou Y., Zhu J., Hu J., Zhang Y., *et al.* (2022) Applicability of Anticancer Drugs for the Triple-Negative Breast Cancer Based on Homologous Recombination Repair Deficiency. *Front Cell Dev Biol* **10**:845950 https://doi.org/10.3389/fcell.2022.845950 | PubMed

[38] **Sanchez-Vega F.,** Mina M., Armenia J., Chatila W.K., Luna A., La K.C., Dimitriadoy S., Liu D.L., Kantheti H.S., Saghafinia S., *et al.* (2018) Oncogenic Signaling Pathways in The Cancer Genome Atlas. *Cell* **173**:321-337. https://doi.org/10.1016/j.cell.2018.03.035 | PubMed

[39] **Healey C.S.,** Dunning A.M., Teare M.D., Chase D., Parker L., Burn J., Chang-Claude J., Mannermaa A., Kataja V., Huntsman D.G., *et al.* (2000) A common variant in BRCA2 is associated with both breast cancer risk and prenatal viability. *Nat Genet* **26**:362-4 https://doi.org/10.1038/81691 | PubMed

[40] **Galkin V.E.,** Esashi F., Yu X., Yang S., West S.C., Egelman E.H. (2005) BRCA2 BRC motifs bind RAD51-DNA filaments. *Proc Natl Acad Sci U S A* **102**:8537-42 https://doi.org/10.1073/pnas.0407266102 | PubMed

[41] **Jimenez-Sainz J.,** Mathew J., Moore G., Lahiri S., Garbarino J., Eder J.P., Rothenberg E., Jensen R.B. (2022) BRCA2 BRC missense variants disrupt RAD51-dependent DNA repair. *eLife* **11** https://doi.org/10.7554/elife.79183 | PubMed

[42] **Adamovich A.I.,** Diabate M., Banerjee T., Nagy G., Smith N., Duncan K., Mendoza Mendoza E., Prida G., Freitas M.A., Starita L.M., *et al.* (2022) The functional impact of BRCA1 BRCT domain variants using multiplexed DNA double-strand break repair assays. *Am J Hum Genet* **109**:618-630 https://doi.org/10.1016/j.ajhg.2022.01.019 | PubMed

[43] **Mangkusaputra V.,** Murachelli A.G., Yu Z., Hollander A.D., Menafra R., Schreuder A., Kloet S.L., Sixma T.K., Noordermeer S.M. (2025) Profiling BRCA1-BRCT interactions and their functional relevance at amino acid resolution. *Nucleic Acids Res* **53** https://doi.org/10.1093/nar/gkaf848 | PubMed

[44] **Xu Z.,** Xie H., Song L., Huang Y., Huang J. (2025) BRCA1 and BRCA2 in DNA damage and replication stress response: Insights into their functions, mechanisms, and implications for cancer treatment. *DNA Repair (Amst)* **150**:103847 https://doi.org/10.1016/j.dnarep.2025.103847 | PubMed

[45] **Tirosh I.,** Venteicher A.S., Hebert C., Escalante L.E., Patel A.P., Yizhak K., Fisher J.M., Rodman C., Mount C., Filbin M.G., *et al.* (2016) Single-cell RNA-seq supports a developmental hierarchy in human oligodendroglioma. *Nature* **539**:309-313 https://doi.org/10.1038/nature20123 | PubMed

[46] **Munkhbaatar E.,** Dietzen M., Agrawal D., Anton M., Jesinghaus M., Boxberg M., Pfarr N., Bidola P., Uhrig S., Hockendorf U., *et al.* (2020) MCL-1 gains occur with high frequency in lung adenocarcinoma and can be targeted therapeutically. *Nat Commun* **11**:4527 https://doi.org/10.1038/s41467-020-18372-1 | PubMed

[47] **Wang Z.,** Wang Y., Chang M., Wang Y., Liu P., Wu J., Wang G., Tang X., Hui X., Liu P., *et al.* (2023) Single-cell transcriptomic analyses provide insights into the cellular origins and drivers of brain metastasis from lung adenocarcinoma. *Neuro Oncol* **25**:1262-1274 https://doi.org/10.1093/neuonc/noad017 | PubMed

[48] **Karasaki T.,** Moore D.A., Veeriah S., Naceur-Lombardelli C., Toncheva A., Magno N., Ward S., Bakir M.A., Watkins T.B.K., Grigoriadis K., *et al.* (2023) Evolutionary characterization of lung adenocarcinoma morphology in TRACERx. *Nat Med* **29**:833-845 https://doi.org/10.1038/s41591-023-02230-w | PubMed

[49] **Moncho-Amor V.,** Ibanez de Caceres I., Bandres E., Martinez-Poveda B., Orgaz J.L., Sanchez-Perez I., Zazo S., Rovira A., Albanell J., Jimenez B., *et al.* (2011) DUSP1/MKP1 promotes angiogenesis, invasion and metastasis in non-small-cell lung cancer. *Oncogene* **30**:668-78 https://doi.org/10.1038/onc.2010.449 | PubMed

[50] **Bayir H.,** Dixon S.J., Tyurina Y.Y., Kellum J.A., Kagan V.E. (2023) Ferroptotic mechanisms and therapeutic targeting of iron metabolism and lipid peroxidation in the kidney. *Nat Rev Nephrol* **19**:315-336 https://doi.org/10.1038/s41581-023-00689-x | PubMed

[51] **Salcedo A.,** Tarabichi M., Buchanan A., Espiritu S.M.G., Zhang H., Zhu K., Ou Yang T.H., Leshchiner I., Anastassiou D., Guan Y., *et al.* (2024) Crowd-sourced benchmarking of single-sample tumor subclonal reconstruction. *Nat Biotechnol* https://doi.org/10.1038/s41587-024-02250-y | PubMed

[52] **Cao J.,** Spielmann M., Qiu X., Huang X., Ibrahim D.M., Hill A.J., Zhang F., Mundlos S., Christiansen L., Steemers F.J., *et al.* (2019) The single-cell transcriptional landscape of mammalian organogenesis. *Nature* **566**:496-502 https://doi.org/10.1038/s41586-019-0969-x | PubMed

[53] **Harding S.M.,** Benci J.L., Irianto J., Discher D.E., Minn A.J., Greenberg R.A. (2017) Mitotic progression following DNA damage enables pattern recognition within micronuclei. *Nature* **548**:466-470 https://doi.org/10.1038/nature23470 | PubMed

[54] **Kwon J.,** Bakhoum S.F. (2020) The Cytosolic DNA-Sensing cGAS-STING Pathway in Cancer. *Cancer Discov* **10**:26-39 https://doi.org/10.1158/2159-8290.cd-19-0761 | PubMed

[55] **Chen Q.,** Sun L., Chen Z.J. (2016) Regulation and function of the cGAS-STING pathway of cytosolic DNA sensing. *Nat Immunol* **17**:1142-9 https://doi.org/10.1038/ni.3558 | PubMed

[56] **Deng Y.,** Xia L., Zhang J., Deng S., Wang M., Wei S., Li K., Lai H., Yang Y., Bai Y., *et al.* (2024) Multicellular ecotypes shape progression of lung adenocarcinoma from ground-glass opacity toward advanced stages. *Cell Rep Med* **5**:101489 https://doi.org/10.1016/j.xcrm.2024.101489 | PubMed

[57] **Li J.,** Zhou C., Gao X., Tan T., Zhang M., Li Y., Chen H., Wang R., Wang B., Liu J., *et al.* (2024) S100A10 promotes cancer metastasis via recruitment of MDSCs within the lungs. *Oncoimmunology* **13**:2381803 https://doi.org/10.1080/2162402x.2024.2381803 | PubMed

[58] **Certo M.,** Tsai C.H., Pucino V., Ho P.C., Mauro C. (2021) Lactate modulation of immune responses in inflammatory versus tumour microenvironments. *Nat Rev Immunol* **21**:151-161 https://doi.org/10.1038/s41577-020-0406-2 | PubMed

[59] **Hu A.,** Sun L., Lin H., Liao Y., Yang H., Mao Y. (2024) Harnessing innate immune pathways for therapeutic advancement in cancer. *Signal Transduct Target Ther* **9**:68 https://doi.org/10.1038/s41392-024-01765-9 | PubMed

[60] **Axelrod M.L.,** Cook R.S., Johnson D.B., Balko J.M. (2019) Biological Consequences of MHC-II Expression by Tumor Cells in Cancer. *Clin Cancer Res* **25**:2392-2402 https://doi.org/10.1158/1078-0432.ccr-18-3200 | PubMed

[61] **Burke K.P.,** Chaudhri A., Freeman G.J., Sharpe A.H. (2024) The B7:CD28 family and friends: Unraveling coinhibitory interactions. *Immunity* **57**:223-244 https://doi.org/10.1016/j.immuni.2024.01.013 | PubMed

[62] **Chi H.,** Pepper M., Thomas P.G. (2024) Principles and therapeutic applications of adaptive immunity. *Cell* **187**:2052-2078 https://doi.org/10.1016/j.cell.2024.03.037 | PubMed

[63] **Kruse B.,** Buzzai A.C., Shridhar N., Braun A.D., Gellert S., Knauth K., Pozniak J., Peters J., Dittmann P., Mengoni M., *et al.* (2023) CD4(+) T cell-induced inflammatory cell death controls immune-evasive tumours. *Nature* **618**:1033-1040 https://doi.org/10.1038/s41586-023-06199-x | PubMed

Liao G, Yang X, Liu Q, Nan S, Liu Y, Li J, Huang S, Ning W, Qin X, Xu G (2025) Molecular architecture of the tumor microenvironment caused by BRCA1 and BRCA2 somatic mutations in lung adenocarcinoma. NCBI Gene Expression Omnibus. ID GSE292700 Go to https://www.ncbi.nlm.nih.gov/geo/query/acc.cgi?acc=GSE292700

Hoadley KA, Yau C, Hinoue T, Wolf DM, Lazar AJ, Drill E, Shen R, Taylor AM, Cherniack AD, Thorsson V, *et al.* (2018) Lung Adenocarcinoma (TCGA, PanCancer Atlas). cBioPortal. ID luad_tcga_pan_can_atlas_2018" https://www.cbioportal.org/study/summary?id=luad_tcga_pan_can_atlas_2018

Chen JB, Yang HC, Teo ASM, LB A (2020) Lung Adenocarcinoma (OncoSG, Nat Genet 2020). cBioPortal. ID luad_oncosg_2020 https://www.cbioportal.org/study/summary?id=luad_oncosg_2020

Peer reviews

Reviewer #1 (Public review):

Summary:

Liao et al. performed a large-scale integrative analysis to explore the function of two cancer genes (BRCA1 and BRCA2) in lung cancer, which is one of the cancers with an extremely high mortality rate. The detailed genetic analysis demonstrated new roles of BRCA1/2 in causing the tumor microenvironment in lung cancer. In particular, the discovery of different mechanisms of BRCA1 and BRCA2 provides an essential foundation for developing drugs that target BRCA1 or BRCA2 in lung cancer therapy.

Strengths:

(1) This study leveraged large-scale genomic and transcriptomic datasets to investigate the prognostic implications of BRCA1/2 mutations in LUAD patients (~2,000 samples). The datasets range from genomics to single-cell RNA-seq to scTCR-seq.

(2) In particular, the scTCR-seq offers a powerful approach for understanding T cell diversity, clonal expansion, and antigen-specific immune responses. Leveraging these data, this study found that BRCA1 mutations were associated with CD8+ Trm expansion, whereas BRCA2 mutations were linked to tumor CD4+ Trm expansion and peripheral T/NK cell cytotoxicity.

(3) This study also performed a comprehensive analysis of genomic variation, gene expression, and clinical data from the TCGA program, which provides an independent validation of the findings from LUAD patients newly collected in this study.

(4) This study provides an exemplary integration analysis using both computational biology and wet bench experiments. The experimental testing in the A549 cell line further supports the robustness of the computational analysis.

(5) The findings of this study offer a comprehensive view of the molecular mechanisms underlying BRCA1 and BRCA2 mutations in LUAD. BRCA1 and BRCA2 are two well-known cancer-related genes in multiple cancers. However, their role in shaping the tumor microenvironment, particularly in lung cancer, is largely unknown.

(6) By focusing on PD-L1-negative LUAD patients, this study demonstrated the molecular mechanisms underlying resistance to immune therapy. These new insights highlight new opportunities for personalized therapeutic strategies to BRCA-driven tumors. For example, they found histone deacetylase (HDAC) inhibitors consistently downregulated 4-R genes in A549 cells.

(7) The deposition of raw single-cell sequencing (including scRNA-seq and scTCR-seq) data will provide an essential data resource for further discovery in this field.

Comments on revisions:

The author has revised accordingly. I have no further comments.

https://doi.org/10.7554/eLife.110662.2.sa2

Reviewer #2 (Public review):

Summary:

This study investigates the impact of BRCA1/2 mutations on immunotherapy in lung adenocarcinoma using multi-omics approaches. The work highlights distinct roles of BRCA1 and BRCA2 mutations in shaping immune-related processes, and is logically structured with clearly presented analyses. However, the conclusions rely primarily on descriptive computational analyses and would benefit from additional immunological validation.

Strengths:

By integrating public datasets with in-house data, this study examines the impact of BRCA1/2 mutations on immunotherapy in lung adenocarcinoma from multiple perspectives using multi-omics approaches. The analyses are diverse in scope, with a clear overall logic and a well-organized structure.

Weaknesses:

The study is largely descriptive and would benefit from additional immunological experiments or validation using in vivo models. The fact that the BRCA1 and BRCA2 samples were each derived from a single patient also limits the robustness of the conclusions.

Comments on revisions:

The authors have addressed my concerns satisfactorily

https://doi.org/10.7554/eLife.110662.2.sa1

Author response:

The following is the authors' response to the original reviews.

> ***eLife Assessment***
>
> *This important study investigates the impact of BRCA1/2 mutations on immunotherapy in lung adenocarcinoma using multi-omics approaches. The detailed genetic analysis of two cancer genes (BRCA1 and BRCA2) demonstrated new roles for these genes in causing the tumor microenvironment in lung cancer. Further experimental explorations of the immune-related changes may still be required. The solid findings of this study provide a foundation for further developing drugs targeting BRCA1/2 in lung cancer therapy.*

We would like to express our sincere gratitude for your thoughtful and constructive comments on our manuscript. We carefully considered each comment from these two reviewers and revised the manuscript accordingly. Below, we provided a point-by-point response to each comment.

> ***Reviewer #1 (Public review):***
>
> *Summary:*
>
> *Liao et al. performed a large-scale integrative analysis to explore the function of two cancer genes (BRCA1 and BRCA2) in lung cancer, which is one of the cancers with an extremely high mortality rate. The detailed genetic analysis demonstrated new roles of BRCA1/2 in causing the tumor microenvironment in lung cancer. In particular, the discovery of different mechanisms of BRCA1 and BRCA2 provides an essential foundation for developing drugs that target BRCA1 or BRCA2 in lung cancer therapy.*
>
> *Strengths:*
>
> *(1) This study leveraged large-scale genomic and transcriptomic datasets to investigate the prognostic implications of BRCA1/2 mutations in LUAD patients (~2,000 samples). The datasets range from genomics to single-cell RNA-seq to scTCR-seq.*
>
> *(2) In particular, the scTCR-seq offers a powerful approach for understanding T cell diversity, clonal expansion, and antigen-specific immune responses. Leveraging these data, this study found that BRCA1 mutations were associated with CD8+ Trm expansion, whereas BRCA2 mutations were linked to tumor CD4+ Trm expansion and peripheral T/NK cell cytotoxicity.*
>
> *(3) This study also performed a comprehensive analysis of genomic variation, gene expression, and clinical data from the TCGA program, which provides an independent validation of the findings from LUAD patients newly collected in this study.*
>
> *(4) This study provides an exemplary integration analysis using both computational biology and wet bench experiments. The experimental testing in the A549 cell line further supports the robustness of the computational analysis.*
>
> *(5) The findings of this study offer a comprehensive view of the molecular mechanisms underlying BRCA1 and BRCA2 mutations in LUAD. BRCA1 and BRCA2 are two well-known cancer-related genes in multiple cancers. However, their role in shaping the tumor microenvironment, particularly in lung cancer, is largely unknown.*

> *(6) By focusing on PD-L1-negative LUAD patients, this study demonstrated the molecular mechanisms underlying resistance to immune therapy. These new insights highlight new opportunities for personalized therapeutic strategies to BRCA-driven tumors. For example, they found histone deacetylase (HDAC) inhibitors consistently downregulated 4-R genes in A549 cells.*
>
> *(7) The deposition of raw single-cell sequencing (including scRNA-seq and scTCR-seq) data will provide an essential data resource for further discovery in this field.*
>
> *Weaknesses:*
>
> *(1) The finding of histone deacetylase (HDAC) inhibitors suggests the potential roles of epigenetic regulation in lung cancer. It would be interesting to explore epigenetic changes in LUAD patients in the future.*

Thank you for your insightful comment. We fully agree that the specific situation of epigenetic dysregulation in LUAD needs to be explored. We believe that future investigations utilizing clinical specimens and animal models to map histone acetylation patterns and DNA methylation profiles were crucial for identifying novel biomarkers and therapeutic targets unique to LUAD.

> *(2) For some methods, more detailed information is needed.*

This is a valid point. We agree that additional details regarding are necessary for clarity and reproducibility. We have expanded these method details in the revised manuscript.

> *(3) There are grammar issues in the text that need to be fixed.*

We apologize for our irregular use of grammar. In the revised manuscript, we carefully checked the grammar and make corrections.

> *(4) Some text in the figures is not labeled well.*

We appreciate the reviewers' comments. We have added labels to the revised version of the figures.

> ***Reviewer #2 (Public review):***
>
> *Summary:*
>
> *This study investigates the impact of BRCA1/2 mutations on immunotherapy in lung adenocarcinoma using multi-omics approaches. The work highlights distinct roles of BRCA1 and BRCA2 mutations in shaping immune-related processes, and is logically structured with clearly presented analyses. However, the conclusions rely primarily on descriptive computational analyses and would benefit from additional immunological validation.*
>
> *Strengths:*
>
> *By integrating public datasets with in-house data, this study examines the impact of BRCA1/2 mutations on immunotherapy in lung adenocarcinoma from multiple perspectives using multi-omics approaches. The analyses are diverse in scope, with a clear overall logic and a well-organized structure.*
>
> *Weaknesses:*
>
> *The study is largely descriptive and would benefit from additional immunological experiments or validation using in vivo models. The fact that the BRCA1 and BRCA2*

> *samples were each derived from a single patient also limits the robustness of the conclusions.*

Thank you for this excellent suggestion. In the revised manuscript, we supplemented the additional immunological experiments and validation based on pathological tissue sections of lung adenocarcinoma patients. In addition, we elaborated on the limitations of our study in the Discussion section and provided reasonable explanations.

> ***Recommendations for the authors:***
>
> ***Reviewer #1 (Recommendations for the authors):***
>
> *(1) The abstract includes a lot of abbreviations, which makes it difficult to follow. For example, "IFN" is not defined. And "HRR" is defined but used only once in the abstract. This issue also appears in other parts, such as "OAK" on page 5, line 114; "DFS" on page 15, line 398; and "DSBs" on page 20, line 558. Please try to avoid unnecessary abbreviations.*

Thank you for highlighting this. We have revised the manuscript to minimize the use of abbreviations. Specifically, we have now defined all necessary abbreviations upon first mention (including 'IFN') and have removed or spelled out those used infrequently to ensure the text flows more smoothly for the reader.

> *(2) Page 5, line 129, what data type is used in this part analysis?*

We apologize for our negligence. The whole exome sequencing data used here has been added in the revised manuscript.

Materials and methods, page 6, lines 131-132: “The raw reads (fastq) of whole exome sequencing were pre-processed and trimmed with fastp (Version: 0.23.4) based on default parameters.”

> *(3) Page 6, line 138, Add citation for ANNOVAR.*

Thank you for your suggestion. We have added a citation for ANNOVAR in the revised manuscript.

> *(4) Page 8, line 211, what cutoff is used to define the significant makers?*

Thank you for your insightful comment. We provided the cutoff used to define significant markers.

Materials and methods, page 8, lines 213-215: “Differential expression genes for specific clusters were identified using the “FindMarkers” function, with a threshold of $|avg\_log2FC| \geq 0.5$ and adjusted P-value ≤ 0.01.”

> *(5) Page 11, line 276, HEK293T is not a lung cancer cell line. It would be better to label the details of this cell line.*

Thank you for your correction. We have now clarified HEK293T in the text by stating: 'human embryonic kidney cell line HEK293T'.

Materials and methods, page 11, lines 277-278: “The human lung cancer cell line A549 (#SCSP-503) and the human embryonic kidney cell line HEK293T (#SCSP-502) were purchased from the Type Culture Collection of the Chinese Academy of Sciences, China.”

> *(6) Page 16, line 415, what samples and how many individuals were used for the exome sequencing?*

We agree that specifying the sample set is crucial. The exome sequencing was conducted on 2 individuals (four samples). The samples used were tumor tissues (2 samples) and matched blood (2 samples). This information has been clarified in the revised manuscript.

Results section, page 16, lines 415-416: “Exome sequencing was performed on four samples from two individuals: two tumor tissues and two matched blood samples.”

> *(7) Page 17, line 468, Replace "Differently" with "In contrast" (more appropriate for scientific writing).*

Thank you for pointing this out. We agree that "In contrast" is more appropriate for scientific writing. Accordingly, we have replaced "Differently" with "In contrast" in this sentence (Results section, page 18, line 483).

> *(8) Page 18, line 489, what is HMG?*

Thank you for pointing this out. HMG stands for High Mobility Group. We have clarified this by writing out the full term upon first mention in the manuscript (Results section, page 19, line 503).

> *(9) Page 19, line 527, check the grammar for this sentence.*

We appreciate your careful reading. We have carefully rephrased this sentence to ensure clarity and grammatical accuracy.

Results section, page 20, line 540: “Based on pseudotime order, we divided trajectories into 10 bins and analyze the activity changes of related features.”

> *(10) Page 20, line 541-546. It would be better to split this long sentence into smaller ones.*

Thank you for your insightful comment. We have revised the text, splitting the long sentence into smaller ones for better clarity.

Results section, page 20, lines 554-559: “MHC class I and II molecules showed increased activity in late pseudotime in *BRCA1*- and *BRCA2*-mutant cells, respectively (Fig. 4G-I). This pattern was also reflected in the cell density analysis (Fig. 4J). Furthermore, $CD8^+$ Tcm and Th1 signatures exhibited higher activity in late pseudotime in *BRCA1*- and *BRCA2*-mutant cells, respectively (Fig. S5F-G). These findings suggest a differential association with $CD8^+$ versus $CD4^+$ T cell engagement.”

> *(11) Page 20, line 550, remove "." after "of".*

Thank you for catching this. We have removed it (Results section, Page 21, line 563).

> *(12) Page 22, line 592, what is "LME"?*

Thank you for pointing this out. "LME" was indeed redundant in the original manuscript, so we have removed it in the revised version (Results section, Page 22, lines 607-609).

> *(13) Page 24, line 674, Replace "suggest" with "suggested"?*

We apologize for our negligence. In the revised manuscript, we have replaced "suggest" with "suggested" (Results section, Page 25, lines 691-693).

> *(14) Page 35, Figure 1I, Use "B cells" instead of "B".*

Thank you for your detailed review. We have changed to the appropriate label in Figure 1I.

> *(15) Page 36, Figure 2H, the statistics and p-value are needed to show.*

Thank you for your suggestion. We have added the statistical analysis for Figure 2H, and the p-values were indicated in the revised Figure.

Special thanks to you for your kind comments.

> ***Reviewer #2 (Recommendations for the authors):***
>
> *Major:*
>
> *(1) Line 44. In the Introduction section, a brief description of the prevalence of HRD or BRCA1/2 mutations in lung cancer patients should be included to highlight the significance of the study.*

This is an excellent suggestion. We revised the Introduction section (page 3, lines 61-64) to include a brief overview of the prevalence of *BRCA1/2* mutations specifically in lung cancer patients. We believe this addition will strengthen the background for readers.

Introduction section, page 3, lines 61-64: "Among the key genetic mutations that drive LUAD, *BRCA1* and *BRCA2* mutations (with prevalence rates of approximately 4% and 5%, respectively) have been increasingly implicated in the pathogenesis and progression of lung cancer [9, 13]."

> *(2) Line 302-355. There are relatively serious grammatical issues, and substantial revision of the text is recommended.*

We acknowledge the grammatical issues in the original text. We have now carefully revised the Materials and methods section of the manuscript (pages 11-14, lines 277-358) to correct these issues and improve the overall readability. We believe the revised version is significantly improved.

> *(3) Line 375. The Results section lacks detailed information on the specific BRCA1/BRCA2 mutations and data explaining how these mutations lead to functional alterations of BRCA1/2.*

Thank you for your insightful comment. In the revised manuscript, we added the amino acid changes caused by the specific *BRCA1/BRCA2* mutation sites and expand the text to discuss the predicted and known pathogenic mechanisms of these variants (Results section, page 16, lines 420-433).

Results section, page 16, lines 420-433: "Exome sequencing data show that these two types of tumor tissues harbor somatic nonsynonymous single nucleotide variants (SNV) in *BRCA2* (p.N372H) and *BRCA1* (p.E991G, p.S1566G, p.K1136R, p.P824L, and p.Y809H), respectively (Table S1). The *BRCA2* p.N372H variant lies within the BRC3 or BRC4 motifs critical for RAD51 binding. It may alter binding affinity, impair high-fidelity homologous recombination repair, and promote genomic instability [39-41]. In *BRCA1*, mutations are distributed across two key functional domains: the Coiled-Coil domain (e.g., p.E991G, p.Y809H, p.P824L) and the BRCT domain (e.g., p.K1136R, p.S1566G). Coiled-Coil mutations disrupt BRCA1-PALB2-BRCA2 complex assembly, impairing localization to DNA damage sites and subsequent *RAD51* recruitment; BRCT domain mutations compromise phospho-protein recognition and G2/M checkpoint control, leading to defective DNA damage response and unchecked proliferation of damaged cells [42-44]. Together, these defects promote the accumulation of genomic scars and chromosomal instability."

> *(4) Line 492-498. Changes in genes associated with BRCA1 and BRCA2 mutations should be validated by immunofluorescence.*

Thank you for your insightful comment. Immunofluorescence would provide valuable orthogonal validation of the protein-level consequences of these mutations. To address this, we obtained pathological tissue sections from patients carrying *BRCA1/2* mutations and performed immunofluorescence staining for *S100A10*, a risk gene associated with *BRCA1* mutations. We found that *S100A10* was upregulated in *BRCA1*-mutated tumor tissue compared to adjacent non-cancerous tissue.

Results section, page 24, lines 673-675: “Immunofluorescence experiments on patient tissue sections revealed that *S100A10* was upregulated in *BRCA1*-mutated tumor tissue relative to adjacent non-cancerous tissue (Fig. S11D-E).”

> *(5) Line 538. Although both BRCA1 and BRCA2 deficiencies impair DNA damage repair, BRCA1, but not BRCA2, activates the cGAS-STING pathway. This is a particularly interesting observation and should be validated by immunofluorescence experiments.*

Thank you for highlighting this observation. To address this, we conducted immunofluorescence experiments to quantify STING, the key protein of cGAS-STING pathway, in *BRCA1*- and *BRCA2*-deficient tissues to confirm this phenotype. We have included these results in the revised manuscript.

Results section, page 21, lines 578-584: “Furthermore, our results revealed that *BRCA1*-mutant tumors showed higher activity of cGAS-STING signaling and STING mediated induction of host immune responses compared to *BRCA2*-mutant tumors (Fig. 5G and Fig. S6F). Also, cGAS-STING signaling gens, including *cGAS*, *STING1*, and downstream factors *STAT1* and *CCL5*, were upregulated in *BRCA1*-mutant tumor cells (Fig. 5H). This observation was validated through immunofluorescence staining experiments on patient tumor tissue sections (Fig. 5I-J).”

> *(6) Line 599. "CD8+ Trm cells were more abundant in BRCA1-mutant sample, whereas CD4+ Trm cells were higher in BRCA2-mutant sample". This part is also recommended to be validated using immunofluorescence or more rigorous flow cytometry analyses.*

We sincerely appreciate this insightful suggestion. To address this, we performed immunofluorescence staining to quantify the abundance of $CD8^+$ and $CD4^+$ Trm cells in *BRCA1*- and *BRCA2*-mutant tissues. We have included these results in the revised manuscript.

Results section, page 22, lines 614-617: We identified two tissue-resident memory T cell (Trm) subsets, $CD8^+$ Trm and $CD4^+$ Trm, both predominantly derived from tumor tissues (Fig. 6B). “Interestingly, our analysis revealed that $CD8^+$ Trm cells were more abundant in *BRCA1*-mutant tumor, whereas $CD4^+$ Trm cells were more abundant in *BRCA2*-mutant tumor (Fig. 6B-D, Fig. S7D, and Fig. S8A-B).”

> *(7) Line 643-676. The authors identified four risk genes associated with BRCA1 mutations-S100A10, LDHA, MYL12A, and GAPDH; however, MYL12A was not validated in the subsequent in vitro experiments. The authors state that "S100A10 can promote cancer metastasis by recruiting MDSC cells, and increased LDHA activity contributes to tumor immune escape." However, because immune cells were not included in the in vitro assays, these results instead suggest that these genes may directly suppress tumor cell proliferation.*

We thank the reviewer for this insightful observation. Our intention was not to suggest that the reduction in proliferation observed in our *in vitro* assays was caused by the disruption of immune cell recruitment or immune escape pathways. As the reviewer correctly points out, those mechanisms are irrelevant in a system lacking immune cells. Our results showing that "Knockdown of *S100A10*, *LDHA*, and *GAPDH* reduced LUAD cell proliferation *in vitro* (Fig. 7D-E)" strongly suggest a direct, cell-autonomous role for these genes in regulating LUAD cell

growth. For the *MYL12A* gene, the existing study have shown that *BRCA1* transcriptionally regulates this gene involved in breast tumorigenesis (PMID: 12032322). In view of the characteristics of *MYL12A* in lung cancer, we will conduct in-depth *in vitro* and *in vivo* validation experiments in future studies.

> *(8) Line 677. The authors should emphasize the limitations arising from the small sample size and the lack of in vivo validation models in the Discussion section.*

Thank you for highlighting these important limitations. We agree that the small sample size and the lack of *in vivo* validation are significant limitations of the current study. We have explicitly addressed these points in the Discussion section (page 27, lines 740-750) to ensure the interpretation of our data is appropriately qualified and to provide transparency regarding the scope of our conclusions.

Discussion section, page 27, lines 740-750: “Although we included both tumor tissues and matched paracancerous and blood samples, the sample size remains modest, which may limit the statistical power and generalizability of our findings. Therefore, our results should be interpreted as preliminary, and further studies with larger, independent cohorts are required to validate these observations. Single-cell RNA-seq and TCR-seq analyses in this study provide high-resolution insights into the cellular and clonal dynamics of the TME, the functional validation of key mechanisms remains largely correlative. While our *in vitro* experiments provide valuable mechanistic insight, the lack of *in vivo* validation, which cannot fully recapitulate the complex TME. Future studies utilizing murine models or patient-derived organoids are essential to establish causal relationships and elucidate the underlying molecular pathways.”

> *Minor:*
>
> *(1) Line 163: cell/μl should be corrected to cells/μL.*

Thank you for catching this. We have corrected it in the revised manuscript (Methods section, page 7, line 165).

> *(2) Line 388: Please clarify how the HRD score, tumor mutation burden, and neoantigen load were calculated.*

We thank the reviewer for this request for clarification. In the revised manuscript, we have expanded the Methods section (page 5, lines 117-121) to provide a detailed description of how these metrics were calculated. HRD score was calculated as the unweighted sum of loss of heterozygosity (LOH), telomeric allelic imbalance (TAI), and large-scale state transitions (LST). Tumor mutation burden (TMB) was defined as the total number of somatic nonsynonymous mutations per megabase of the exome captured by the sequencing panel. Neoantigen load was predicted by NetMHCpan using the patient's HLA typing and the identified somatic mutations. The data for these three indicators all obtained from a previous study (PMID: 29628290). We believe these additions provide the necessary transparency and reproducibility for our study.

Methods section, page 5, lines 117-121: The HRD score was determined by summing specific genomic alterations, including loss of heterozygosity (LOH), large-scale state transitions (LST), and telomeric allelic imbalances (TAI). “Tumor mutation burden (TMB) was defined as the total number of somatic nonsynonymous mutations per megabase of the exome captured by the sequencing panel. Neoantigen load was predicted by NetMHCpan using the patient's HLA typing and the identified somatic mutations.”

> *(3) Line 421: BRCA12 should be corrected to BRCA2.*

Thank you for your detailed review. We have revised it.

> *(4) The order of Figures 7D and 7E should be reversed.*

Thank you for your insightful comment. According to your suggestion, we reversed the order of Figures 7D and 7E in the revised manuscript.

Special thanks to you for your kind comments.

https://doi.org/10.7554/eLife.110662.2.sa0